BULGARIAN ACADEMY OF SCIENCES

INSTITUTE OF OPTICAL MATERIALS AND TECHNOLOGIES

"ACAD. YORDAN MALINOVSKI"

Abstract

of a dissertation for the award of the educational and scientific degree "doctor"

SYNTHESIS OF NANOLAYERS OF 2D MATERIALS FOR APPLICATIONS IN OPTOELECTRONICS

NIKOLAY DIYANOV MINEV

Professional field 4.1. Physical Sciences
Doctoral program "Electrical, optical and magnetic properties of condensed matter"

SCIENTIFIC SUPERVISOR: Prof. Dr. Vera Marinova

Sofia, 2026

Introduction

Two-dimensional inorganic materials, such as graphene, black phosphorus (BP), hexagonal boron nitride (h-BN), and transition metal dichalcogenides (TMDCs), with the chemical formula MX_2, where M is a transition metal (Mo, W, etc.) and X is a chalcogen (S, Se, or Te), are among the most promising class of ultrathin layered 2D nanomaterials that meet modern technological requirements.

2D materials are characterized by strong covalent bonds within a single layer and weak Van der Waals interactions between adjacent layers, which makes them extremely easy to exfoliate. Separated layer by layer, they have the unique ability to maintain their structural integrity down to an atomic layer thickness, and depending on the thickness (number of layers) and chemical composition, their properties can range from conductive to insulating; from transparent to opaque; from mechanically rigid to elastic. In this aspect, 2D materials emerge as one of the most promising building blocks for modern optoelectronics, providing a full range of material types, including insulators, semiconductors and semi-metals, depending on the width of their band gap. This defines them as one of the most promising candidates for the next generation of materials for optics, optoelectronics and photonics.

Currently, the chemical vapor deposition (CVD) method is the most developed and offers enormous possibilities for the direct synthesis of large-area 2D materials. Direct synthesis on insulating substrates would enable the production of atomically thin transistors, photodetectors, ultrathin and flexible elements for next-generation optics, miniaturized elements for sensors and spintronics, all without the need for layer transfer.

However, obtaining TMDCs nanolayers with controllable thickness and reproducible optical and electrical properties is an extremely challenging task, confirmed by active scientific and technological research worldwide.

RELEVANCE, PURPOSE AND STRUCTURE OF THE DISSERTATION

The rapid development of modern electronic, information and communication technologies requires a continuous search for new concepts for creating faster, more compact and energy-efficient electronic and optoelectronic components. Traditional silicon-based electronics are rapidly approaching their fundamental limitations, which necessitates the transition to new classes of materials. In this context, two-dimensional (2D) materials are emerging as one of the most important alternatives for the next generation of optoelectronic devices.

The relevance of the dissertation work, aimed at obtaining nanoscale layers of 2D materials for optoelectronics, is determined by the following key factors:

- **Excellent optical and electronic properties:** In contrast to their bulk counterparts, 2D materials (such as transition metal chalcogenides, black phosphorus, hexagonal boron nitride, etc.) demonstrate strongly pronounced quantum effects. The transition from an indirect to a direct band gap upon thinning to a monolayer (e.g., in MoS_2) leads to extremely strong interaction with light, strong photoluminescence, and excellent charge carrier mobility. This makes them suitable for creating ultrasensitive photodetectors, light-emitting diodes, and solar cells.
- **Need for flexible and transparent optoelectronics:** The atomic thickness of 2D materials gives them exceptional mechanical flexibility and optical transparency. This opens up possibilities for wearable electronics, flexible displays, integrated sensors in smart clothing, and biocompatible implants—applications where conventional solid semiconductors are impractical.
- **Need for reproducible and controllable preparation methods:** Despite theoretical and experimental progress, the main barrier to the industrial commercialization of 2D materials remains their scalable, controllable and reproducible preparation. Most studies rely on mechanical exfoliation, which is not applicable for mass production. The development and optimization of methods for obtaining high-quality nanoscale layers over a large area (by chemical vapor deposition - CVD, atomic layer deposition - ALD, MOCVD, MBE, etc.) remains a scientific and technological problem.

In summary, developing new technologies and improving existing ones for the synthesis of 2D materials is a fundamental step toward realizing their enormous potential in optoelectronics. This

dissertation addresses the relationship between fundamental knowledge and real-world technological applications, making this research relevant, timely, and highly innovative.

The goal of this dissertation is to establish the optimal conditions for the synthesis of noble transition metal dichalcogenides and to investigate their properties for optoelectronic applications.

To achieve this goal, the following main tasks have been established for this dissertation:

1. To synthesize nanoscale layers of noble transition metal dichalcogenides using chemical vapor deposition (CVD) and thermally assisted conversion (TAC) methods.
2. To investigate the structural, optical, and electro-optical properties of the synthesized materials.
3. To demonstrate optoelectronic applications for the resulting nanoscale layers.

The subjects of research in this dissertation are transition metal dichalcogenides (TMDCs), specifically those based on noble metals such as Pt and Pd. This work focuses on finding conditions for their reproducible preparation using methods such as thermally assisted conversion (TAC) and chemical vapor deposition (CVD) with solid and liquid precursors, followed by characterization with various analytical techniques. Crucially, noble metal-based TMDCs are extremely stable under atmospheric conditions. This chemical inertness makes them much more practical for the fabrication of chips and sensors. Furthermore, these materials combine the electronic properties of 2D semiconductors with the superior catalytic and electronic activity of noble metals. Therefore, the main goal of this dissertation is to study the influence of technological parameters (temperature, pressure, gas flow rate, and precursor type) on the synthesis of TMDC layers, aiming to achieve the controllable growth of single- and multi-layer structures with high spatial homogeneity over large areas.

The dissertation includes

Chapter One presents a Literature Review dedicated to two-dimensional (2D) materials and their applications in optics and optoelectronics. The chapter contains a brief description of two-dimensional materials as a new class of nanomaterials, their basic physical and chemical properties, and discusses their advantages and disadvantages. Main attention is paid to transition noble metal dichalcogenides and their applications in optoelectronics, sensors, and photonics.

The second chapter presents the main methods for obtaining 2D materials such as: exfoliation from a bulk crystal (mechanical exfoliation), liquid phase exfoliation, atomic layer deposition, thermally assisted conversion (TAC), molecular beam epitaxy, chemical vapor deposition (CVD) and metal-organic chemical vapor deposition (MOCVD).

The third chapter is dedicated to the techniques used for analysis such as: Optical microscopy, X-ray photoelectron spectroscopy, Raman spectroscopy, Ellipsometry, Atomic force microscopy, Transmission electron microscopy, XRD analysis and others.

Chapter Four is Experimental and is dedicated to the preparation and characterization of transition metal dichalcogenides: platinum diselenide ($PtSe_2$) and ditelluride ($PtTe_2$) by Chemical Vapor Deposition (CVD), Thermally Assisted Conversion (TAC) and synthesis with liquid precursors. Details and discussion on the preparation and characterization of bulk crystals of $PdSe_2$ are also presented .

The fifth chapter is dedicated to the application of selected, synthesized nanolayers of noble transition metal dichalcogenides as: antibacterial coatings against *Escherichia coli*, transparent conductive layers in polymer-dispersed liquid crystal devices for near-infrared light switches, and active elements in field-effect transistors.

The dissertation concludes with a summary of the major original contributions, followed by the author's related publications, current citation metrics, and a record of relevant conference presentations and project participations.

I Synthesis of noble transition metal dichalcogenides (NTMDCs): $PtSe_2$, $PtTe_2$ and $PdSe_2$

I.1 Synthesis of platinum selenides and tellurides ($PtSe_2$ and $PtTe_2$) by TAC method

The development of a recipe for the synthesis of platinum selenides and tellurides by the TAC method requires systematic optimization of several key process parameters, such as temperature, gas mixture flow rate, reaction time, and temperature ramp rate. These parameters have a strong influence on the kinetics of selenization/tellurization, crystal quality, and final layer morphology. By carefully tuning the TAC synthesis conditions, it is possible to achieve controlled conversion of Pt to $PtSe_2$ and $PtTe_2$ with the desired layer thickness and crystallinity.

During the recipe development process, temperature, time and gas flow were varied. This allowed us to establish that a temperature of 500 °C, a flow of 150 [sccm] and a synthesis time of 2 h were the optimal conditions for obtaining both $PtSe_2$ and $PtTe_2$ layers on several types of substrates - glass (soda lime), quartz (fused silica) and silicon/silicon oxide (Si/SiO_2).

Both dichalcogenides were synthesized by direct selenization/tellurization of a previously deposited platinum (Pt) layer by magnetron sputtering. The selenization (or tellurization) was carried out in a horizontal quartz tube CVD reactor with three independent temperature zones. For this process, we used ultra-high purity Se (or Te) as a source of chalcogenide vapors.

The first step in the synthesis by the TAC method involves the deposition of a thin Pt layer by magnetron sputtering using a Pt target (a RF magnetron sputtering system (13.56 MHz) was used) onto a soda-lime glass at three different Pt deposition times, 3, 6 and 10 seconds, respectively. The Pt layer deposition process requires careful control to achieve the desired morphology and ensure consistency in the subsequent selenization steps. The applied magnetron sputtering power is 300 W, and the pressure is fixed at 6×10^{-1} torr for the three Pt deposition times.

The second step is the selenization/tellurization (i.e. the addition of the corresponding chalcogen), which consists in placing the thus obtained Pt layers in a three-zone CVD reactor. The Pt-coated substrates are positioned in the thermal plateau of the central temperature zone (~ 500 ° C), while the Se evaporation source is placed in a quartz crucible in the low temperature/upper zone (~ 280 ° C). The process is catalyzed with a reactive mixture of carrier gases Ar (90%) / H_2

(10%) at a flow rate of 150 sccm. Similarly, the cooling rate is also chosen to prevent any possible loss of Se from the sample. The third zone of the furnace is set at 530 ° C to provide a more uniform thermal gradient. Heating rates of 16.5 ° C /min (Se zone or evaporation zone) and 27.8 ° C /min (Pt /glass zone or fusion zone) are synchronized to simultaneously reach operating temperatures of 280 °C and 500 °C (required for evaporation/reaction). The addition of small amounts of hydrogen facilitates the formation of intermediate tellurium (selenium) compounds - for example, H_2Te (H_2Se), which react more easily with platinum. In addition, the same gas mixture is also used to purge the quartz tube to eliminate excess oxygen, which provides controlled growth conditions. The synthesis time is 2 hours at atmospheric pressure. After completion of the procedure, the furnace/reactor is turned off for natural cooling to room temperature. The temperature diagrams for the preparation of $PtSe_2$ and $PtTe_2$ are presented in Fig. 1a and Fig . 2b

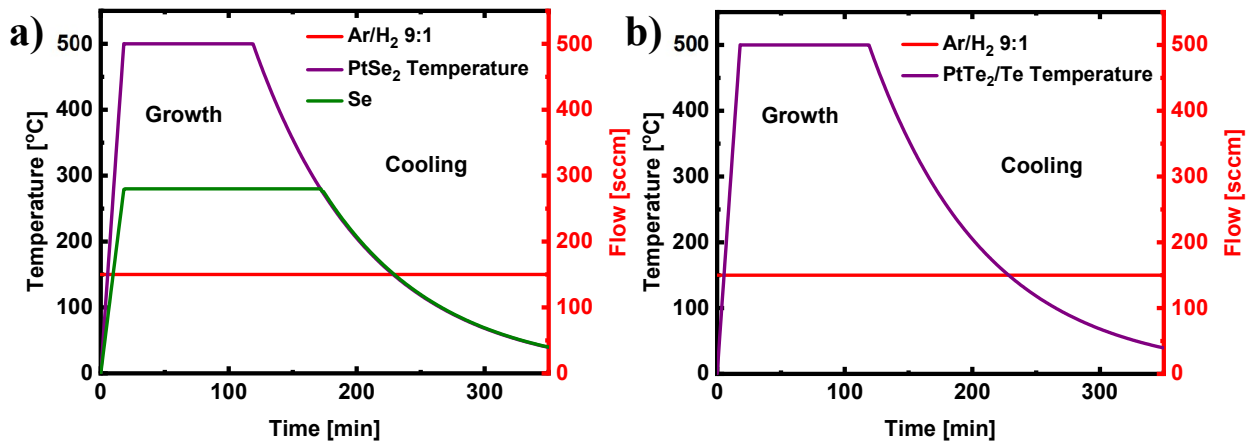

Figure 1 (a) Temperature profile for the synthesis of $PtSe_2$ via TAC, (b) Temperature profile for the synthesis of $PtTe_2$ via TAC

The successful synthesis of the samples was confirmed by Raman analysis presented in Fig. 2a and Fig. 2b. The positions of the two Raman active modes E_g and A_{1g} respectively 177 cm $^{-1}$ (114 cm $^{-1}$) and 208 cm $^{-1}$ (156 cm $^{-1}$) for $PtSe_2$ ($PtTe_2$) match well with the data reported in the literature for both materials [1,2]

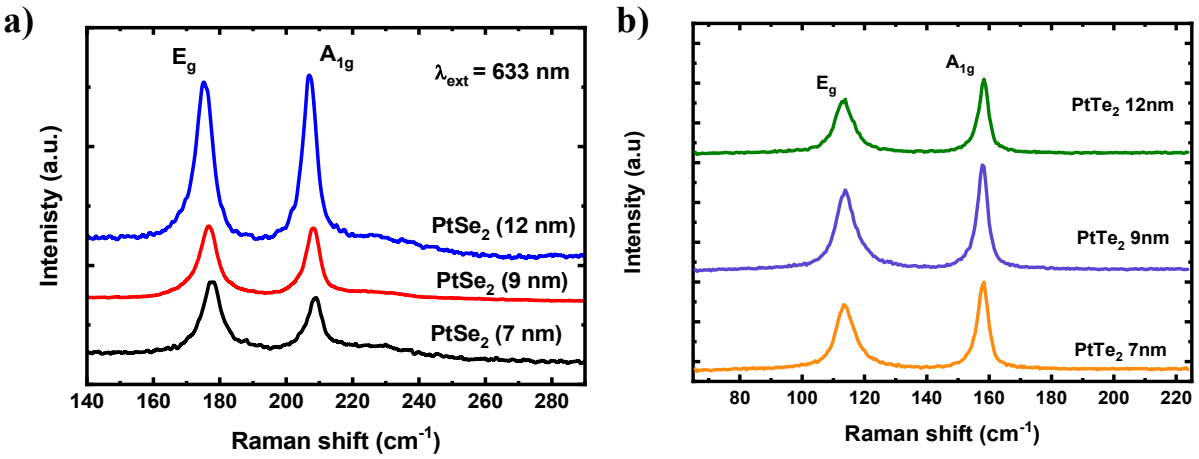

Figure 2 Raman spectra of $PtSe_2$ (a) and $PtTe_2$ (b) taken using red (633 nm) excitation wavelength**.**

To characterize the microstructure and phase composition of the Pt layers after their selenization, TEM analysis was performed, providing key insights into the structural integrity and crystallinity. TEM analysis provides information on the influence of the synthesis process on the final material properties, allowing for potential optimization in future studies.

TEM micrographs of the samples $PtSe_2$ with the three different deposition times of the Pt layer (Fig. 3 a, d, g) show that the thinnest layer is mostly discontinuous, while the other two cover the substrate relatively evenly. The performed analyses show that with decreasing thickness, achieving a continuous layer becomes more challenging, affecting the electrical and optical properties. All three layers show the typical polycrystalline morphology, characterized by randomly oriented crystal grains, consistent with the deposition method. Indexing of the diffraction peaks (Fig. 3b, e, h) allowed us to determine the phase composition of the layers. A trigonal phase of $PtSe_2$ with space group $P\bar{3}m1$ and lattice parameters a = 3.72400 Å and c = 5.06200 Å (COD entry #96-900-9118) was identified, which was also confirmed for the chemical composition of

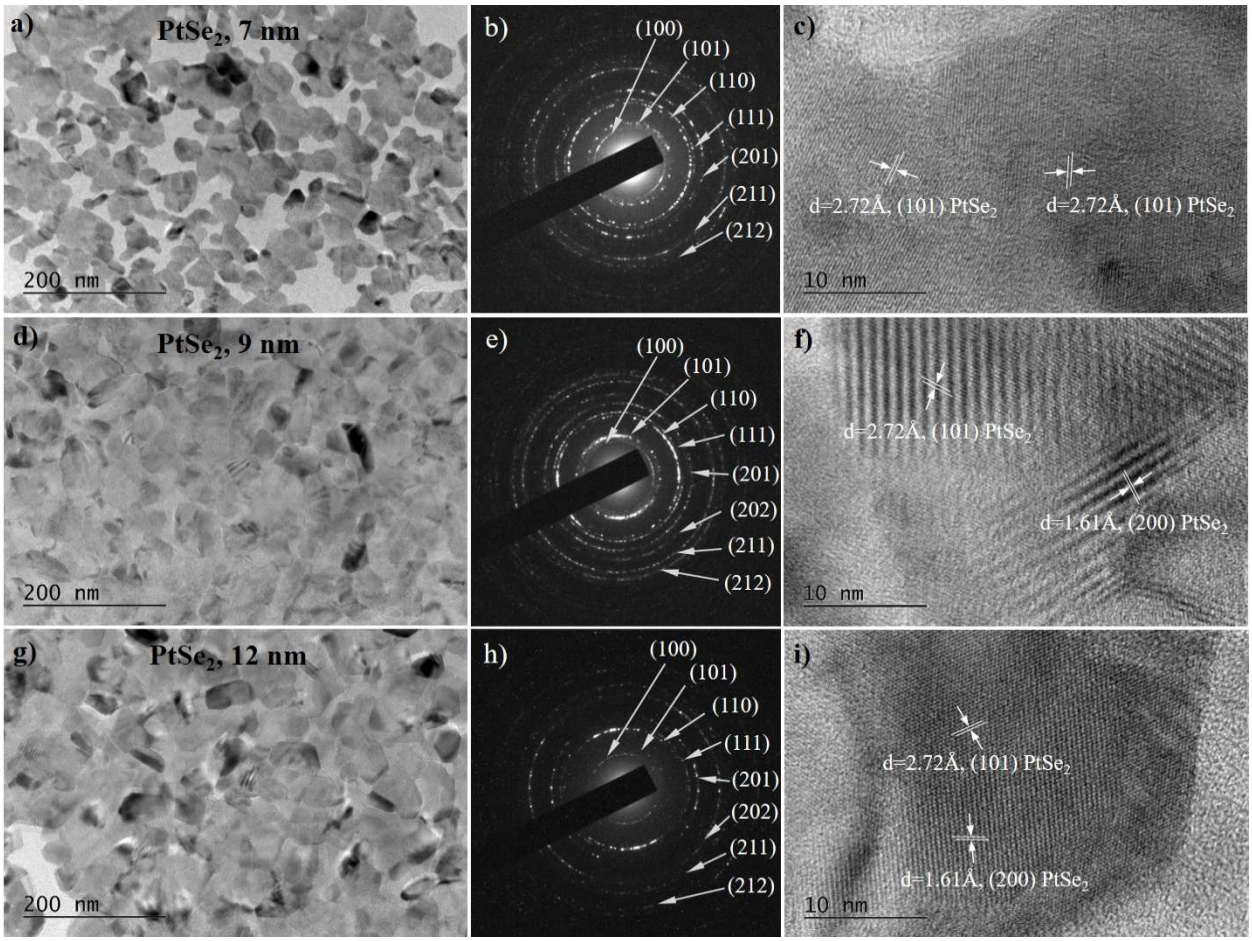

Figure 3 TEM analysis at 40,000× magnification of $PtSe_2$ layers of 7 nm (a), 9 nm (d), and 12 nm (g); electron diffraction from a selected region of $PtSe_2$-7 nm b), $PtSe_2$-9 nm e), and $PtSe_2$-12 nm h) layers; and HRTEM images of $PtSe_2$-7 nm c), $PtSe_2$-9 nm f), and $PtSe_2$-12 nm i) layers.

the layers surfaces by XPS analysis . This phase identification is crucial for verifying the successful formation of the $PtSe_2$ structure and its potential electronic properties.

Information on the morphological and phase composition of the TAC-synthesized $PtTe_2$ was obtained from TEM analysis. Fig. 4 shows micrographs of a 12 nm thick $PtTe_2$ layer, synthesized on a glass substrate. Figure 4a shows a region captured at 40000x magnification, where the well-formed boundaries between individual crystallites are clearly visible, confirming the polycrystalline nature of the layer. Figure 4c shows the boundary between two adjacent

crystallites in high resolution mode. Planes with interplanar distances of 1.65Å and 1.73Å are clearly visible, which correspond to the crystallographic planes (201) and (200) of $PtTe_2$.

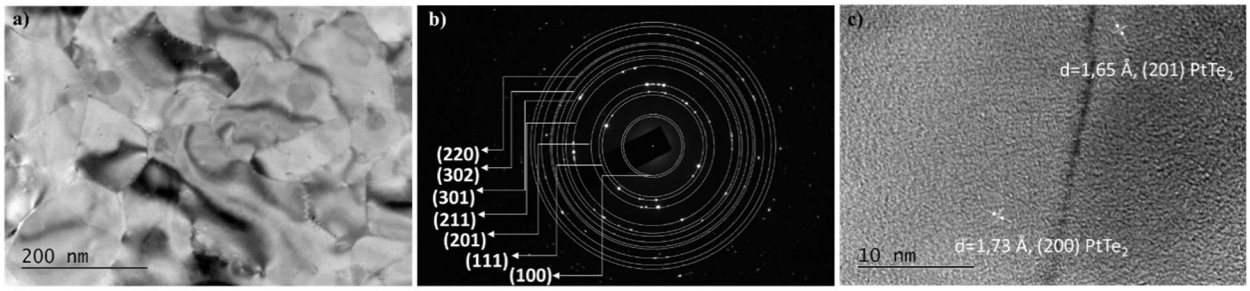

Figure 4 TEM analysis of transferred 2D $PtTe_2$. a) at 40k magnification, b) selected area electron diffraction (SAED) pattern with labeled planes, and c) high-resolution image with calculated interplanar distances

Selected area diffraction (Fig. 4 b) allowed the exact phase composition of the sample to be determined. A trigonal phase of $PtTe_2$ was found. with a space group of symmetry $P\bar{3}m1$ and crystal lattice parameters a = 4.01800 Å and c = 5.21200 Å (COD # 96-153-9202).

Using the Tauc − Lorentz oscillatory model the complex permittivity, $\varepsilon\hat{} = \varepsilon_1 + \varepsilon_2$ and the optical constants of a $PtSe_2$ nanolayer were calculated . The model proposed by Jellison and Modine [3] is a combination of Tauc's law [4] which describes the spectral dependence of the absorption threshold in the case of indirect allowed transitions and the Lorentz oscillator model used in the case of electron transitions from the valence to the conduction band. The model gives an expression for the imaginary part, ε_2, of the dielectric function if only one transition is considered.

$$\varepsilon_2 = \frac{\mathrm{AE_0}\Gamma\left(\mathrm{E}-\mathrm{E}_g\right)^2}{((E^2-E_0^2)^2+\ \Gamma^2E^2)}\ \frac{1}{E} \qquad for\ E > E_g$$

$$\varepsilon_2 = 0 \qquad for\ E \le E_g \tag{1}$$

where E_g is the optical band gap . In the Tauc-Lorentz model, this is expressed as the photon energy at which absorption becomes zero ($\varepsilon_2 = 0$). E_0 is the energy of the maximum transition probability or the position of the absorption peak, Γ is the broadening parameter or damping coefficient

associated with the full width at half maximum of the absorption peak a, and A is the intensity of the absorption peak, which depends on the matrix elements of the optical transition.

The real part of the dielectric function ε_1 is obtained by Kramers-Kronig integration of ε_2 :

$$\varepsilon_1 = \varepsilon_\infty + \frac{\frac{2}{\pi} P \int_{E_g}^{\infty} \xi \varepsilon_2(\xi)\, d\xi}{\xi^2 - E^2} \tag{2}$$

The real and imaginary parts ε_1 and ε_2, of the complex permittivity are related to the refractive index n and the absorption index, k, by the following equations

$$n = \sqrt{\frac{\sqrt{\varepsilon_1^2 + \varepsilon_2^2} + \varepsilon_1}{2}} \tag{3}$$

$$k = \sqrt{\frac{\sqrt{\varepsilon_1^2 + \varepsilon_2^2} - \varepsilon_1}{2}} \tag{4}$$

The dispersion of the refractive index and the absorption index are presented in Fig. 5a–f. As can be seen, the refractive index (n) values increase with increasing thickness throughout the studied spectral range of 200–2100 nm. At wavelengths shorter than 1000 nm (λ< 1000 nm), the refractive index exhibits anomalous dispersion. This behavior is most likely due to generated excitons in $PtSe_2$.

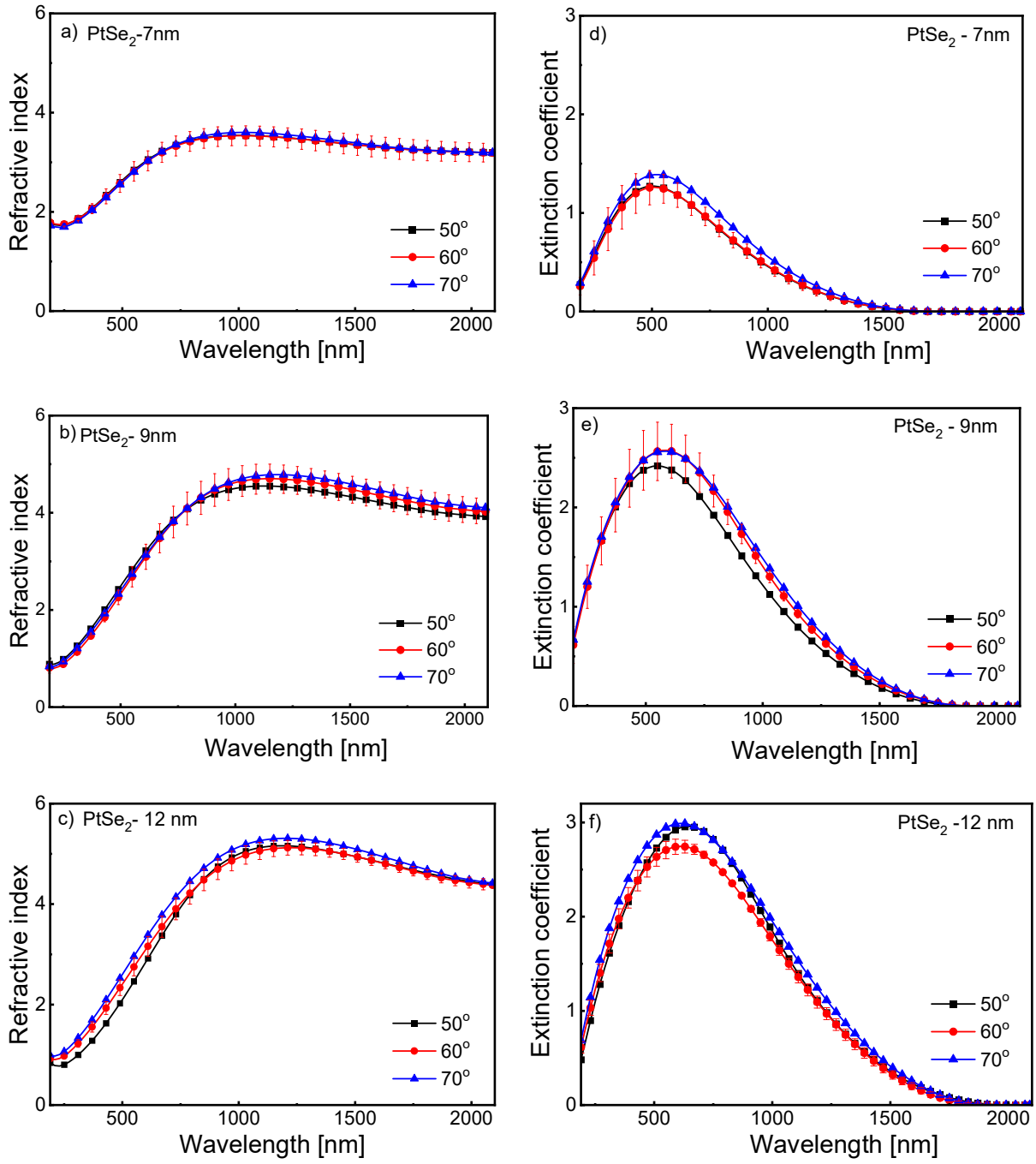

Figure 5 Ellipsometric data from $PtSe_2$ obtained by TAC. (a−f) Dispersions of the refractive index and absorption coefficient of thin $PtSe_2$ films of various thicknesses, calculated from ellipsometric measurements at incident angles of 50°, 60°, and 70°.

Depending on the layer thickness, the refractive index n reaches its maximum values in the spectral range 1000−1200 nm. The position of the maximum shifts from 1030 to 1190 nm, while the maximum value of n decreases from 5.12 to 3.61 with decreasing layer thickness. A significant decrease in the values of n is observed between 1200 nm and 2100 nm. with decreasing layer thickness. Reducing the thickness from 12 nm to 9 nm leads to a decrease in n from 4.42 to 4.28 at a wavelength of λ = 1700 nm. These values are higher than those reported in the literature [5] for $PtSe_2$ with a thickness of 7.5 nm. Further reduction of the thickness of the thin layers to d ~ 7 nm leads to a significant larger changes in the refractive index, with the value for n for the same wavelength being 3.28. The calculated values of k show that the extinction decreases with decreasing thickness throughout the studied spectral range (Fig. 5). In the spectral range of 200−1600 nm, a large absorption is observed in the absorption spectrum. The position of the maximum value of k shifts to shorter wavelengths with decreasing layer thickness, while the maximum values of k are decreasing.

I.2 Synthesis of $PtSe_2$ by CVD

The synthesis of platinum diselenide ($PtSe_2$) by chemical vapor deposition (CVD) has also emerged as a reliable method for the synthesis of high-quality, thin films of transition metal dichalcogenides over a large area.

For the synthesis of $PtSe_2$, $PtCl_2$ was used as the Pt source, and Se in the form of capsules was used for the generation of chalcogenide vapors. At one end of the CVD reactor, in the direction of the gas flow, 1g of Se was placed in a quartz holder. 30 mg of $PtCl_2$ were placed 10 cm from the selenium in close proximity to glass substrates (Fig. 6a). The amount of selenium used ensured a stable vapor flow during the synthesis. The samples were then placed in a quartz tube furnace, with two independent temperature zones, where selenium was placed in the low temperature zone to generate vapor, and $PtCl_2$ and substrates were placed in the high temperature zone. During the next 20 min, the tube was purged with Ar at a pressure of 2 torr and a temperature of 100 $^\circ$C to remove moisture and oxygen. The synthesis proceeded at a flow of 200 sccm Ar and a temperature of 500 $^\circ$C for 5 min at low pressure (Fig. 6b) . The layer thickness could be adjusted by controlling the amount of $PtCl_2$ during the synthesis, the distance between the precursor and the substrates, or

the deposition time. Glass substrates, as in the TAC method, proved to be suitable for the preparation of $PtSe_2$, as they are a source of Na, which favors the growth of the layer.

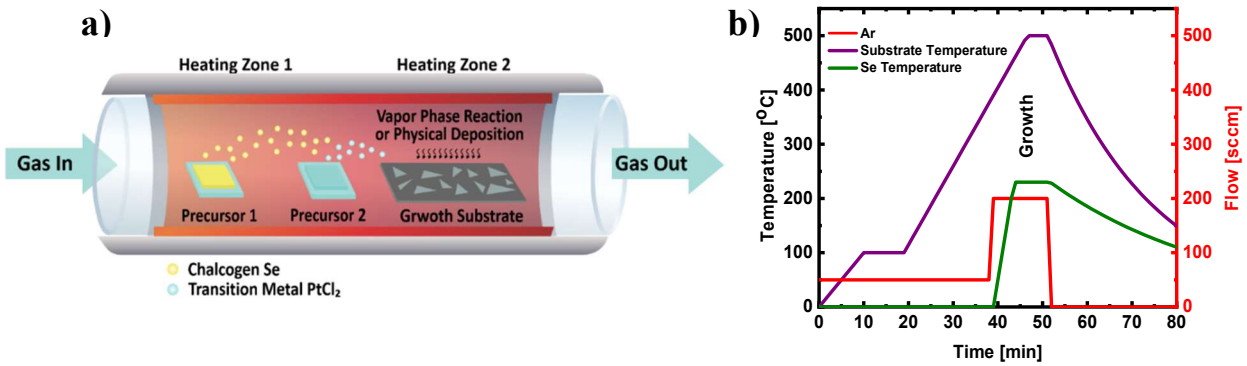

Figure 6 a) Schematic of $PtSe_2$ synthesis by CVD. b) Temperature profile of the process

The $PtSe_2$ layers synthesized on glass were investigated with Raman spectroscopy. Fig. 7 shows the result of the measurement where the typical A_{1g} and E_g vibrational modes of 2D are clearly visible. $PtSe_2$ along with a clearly pronounced shoulder at 230–235 cm $^{-1,}$ characteristic of thin samples [2] .

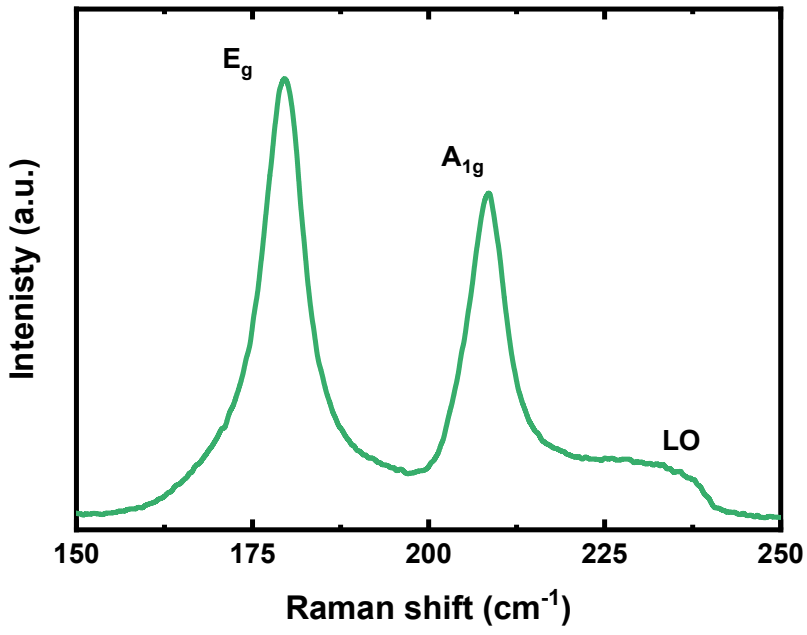

Figure 7 Raman spectrum of $PtSe_2$ synthesized by CVD on glass substrates, showing the characteristic A_{1g} and E_g vibrational modes of $PtSe_2$

I.3 Synthesis of $PtSe_2$ with liquid precursors

Another way to synthesize $PtSe_2$ layers is by using a liquid precursor for Pt. The use of liquid precursors in the synthesis of transition metal dichalcogenides offers several significant advantages. Liquid-phase methods often operate at lower temperatures and can use less expensive equipment compared to high-temperature vapor-phase deposition methods. This makes them attractive for large-scale production from an economic point of view. Furthermore, liquid-phase methods can be more environmentally friendly, as the need for hazardous gases and high-energy processes can be reduced. The liquid phase facilitates the growth of TMDCs heterostructures, where different TMDC materials are stacked on top of each other. This capability is essential for the development of electronic and optoelectronic devices. For example, two-step methods for depositing two different precursors have been used to synthesize TMDCs heterostructures with controlled composition and properties. Liquid-phase precursors also allow the creation of doped TMDCs by simply mixing different dissolved precursors. This flexibility is useful for the synthesis of TMDCs with selected compositions and tunable electronic and optical properties that meet specific application requirements [6,7] .

For synthesis of $PtSe_2$ a liquid precursor was prepared according to the following recipe: 0.1 [g] of powdered $PtCl_2$ was mixed with 0.01 [g] NaCl, 10 [ml] ethanol, 1 [ml] deionized water and 200 [µl] hydrochloric acid (HCl). Then the solution containing Pt was applied by centrifugation at 4000 rpm for 1 minute onto a glass substrate (Fig. 8a) and subsequently selenized at a temperature of 500 $^{\circ}$C for 2 hours. The resulting layers were examined by Raman spectroscopy Fig. 8 b), which confirmed the successful synthesis.

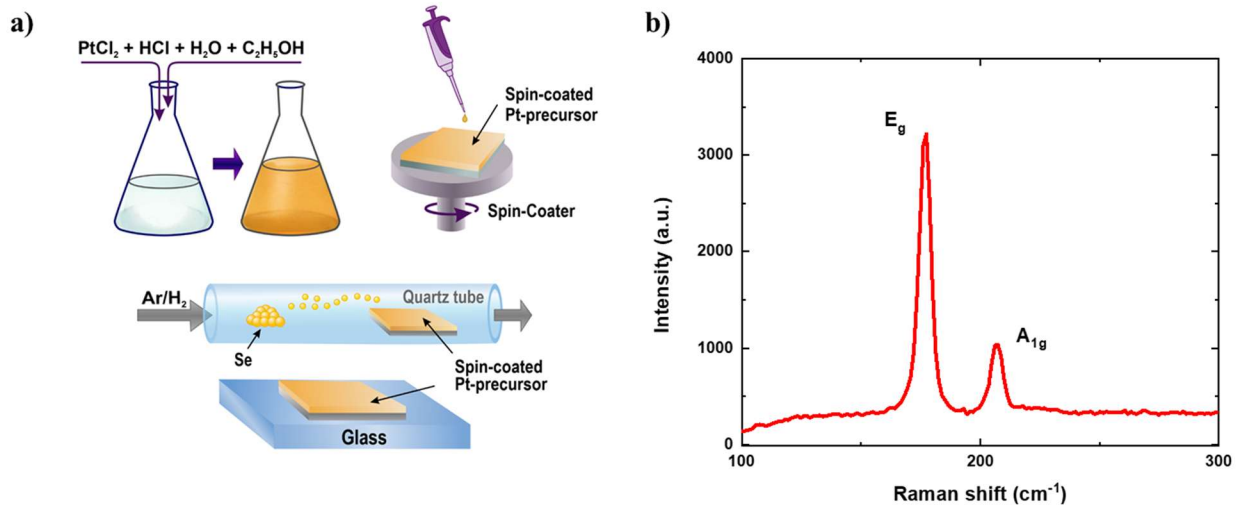

Figure 8 a) Synthesis of $PtSe_2$ using liquid precursors b) Raman spectroscopy of $PtSe_2$ synthesized using liquid precursors, showing the characteristic A_{1g} and E_g vibrational modes of $PtSe_2$

CVD synthesis and analyses of $PdSe_2$

Palladium diselenide ($PdSe_2$) is an important representative of the transition metal dichalcogenides with a layer dependent band gap and an extremely high potential for applications in electronic and optoelectronic devices. However, the availability of high-quality crystals with large area and controlled phase is still a challenge. The controlled synthesis of high-quality $PdSe_2$ enables a wide range of additional integrated optical and electro-optical applications .

The preparation of $PdSe_2$ by chemical vapor deposition (CVD), similar to $PtSe_2$, is also a reliable method for the synthesis of high-quality, thin films. For the synthesis of $PdSe_2$, $PdCl_2$ was used as the Pd source, and Se in the form of capsules was used to generate the chalcogenide vapor. In such a synthesis, 1g of Se is placed at one end of the CVD reactor (in a quartz holder), located in the direction of the gas flow. 30 mg of $PdCl_2$ were placed 10 cm from the selenium, located in close proximity to cleaned glass substrates (Fig. 9a).

The loading of the CVD reactor with the precursors is the same as for $PtSe_2$. The synthesis takes place at a flow of 200 sccm Ar and a temperature of 500 ^{o}C for 5 minutes at a pressure of 500 torr (Fig. 9b). Glass substrates proved to be suitable for obtaining $PdSe_2$, as they are a source of Na, which favors the growth of the layer .

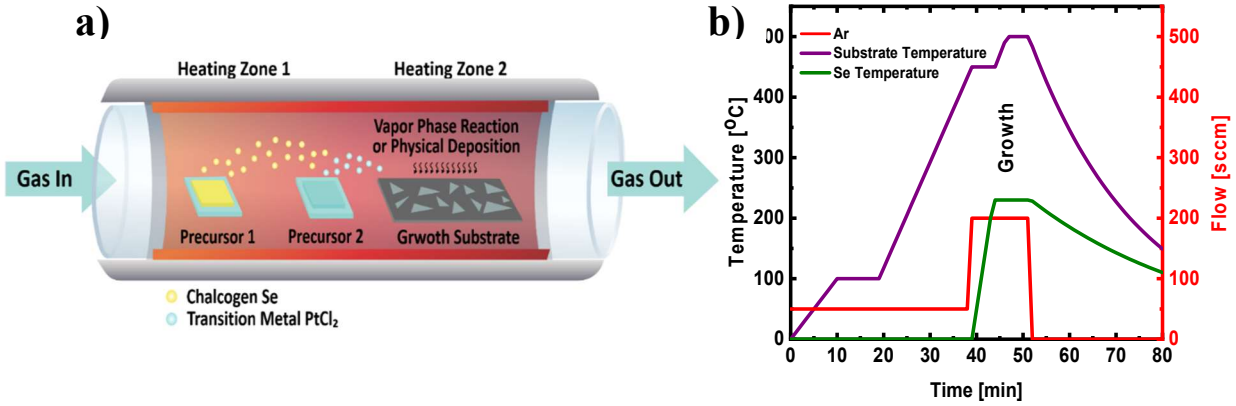

Figure 9 a) Synthesis of $PdSe_2$ by CVD. b) Temperature profile of the process.

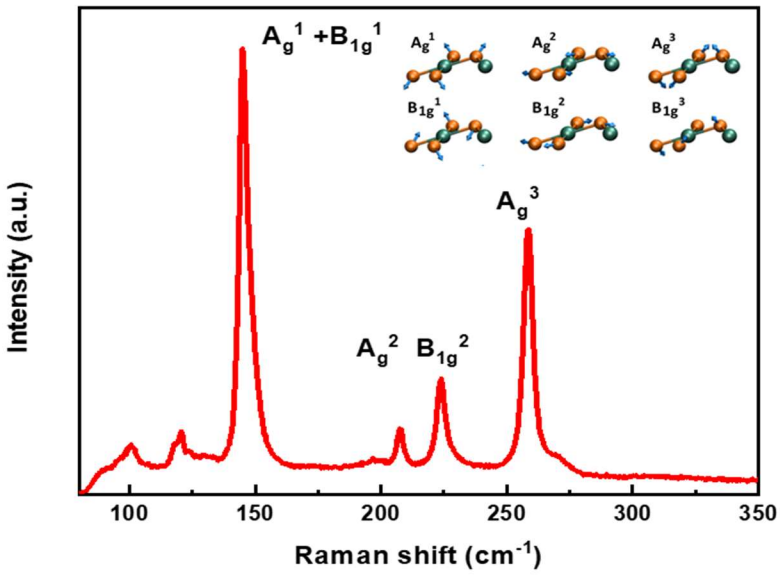

Figure 10 Raman spectrum of $PdSe_2$ synthesized by CVD and the six active Raman modes.

Raman spectroscopy was used to confirm the formation and structural quality of $PdSe_2$. Due to its low-symmetry orthorhombic crystal structure, $PdSe_2$ exhibits several Raman-active

vibrational modes. Fig. 10 shows the Raman spectrum of thin $PdSe_2$ with the characteristic vibrational modes of 14 5, 207.6, 224 and 258.5 cm^{-1} corresponding to $A_g^1 + B_{1g}^1$, A_g^2, B_{1g}^2 and A_g^3 . These values are in good agreement with the literature [8] .

I.4 Synthesis of 3D (bulk) single crystal $PdSe_2$

Single crystals of $PdSe_2$ were prepared by the flux method (high-temperature solution), with selenium (Se) used as the solvent/flux (Fig. 11a). Due to the high vapor pressure of Se and the exothermic nature of the reaction between the two elements, quartz ampoules with the following parameters were used: wall thickness: 3 mm, diameter: 20 mm; length: 100 mm.

A preliminary solid-phase synthesis of the compound $PdSe_2$ was performed. Pd powder (99.98%, Alfa Aesar) and Se powder (99.94%, Alfa Aesar) in stoichiometric amounts were used as starting materials. After homogenization of the mixture, the ampoules were evacuated to ~10^{-5} torr and sealed. The synthesis was carried out in a furnace with a controlled temperature increase at a rate of 20 °C/h to 850 °C, with the samples being kept at this temperature for 4 days. The system was then cooled at a rate of 40 °C/h, and the resulting polycrystalline $PdSe_2$ was ground and homogenized in an agate ball mill to ensure uniform distribution of the constituent elements.

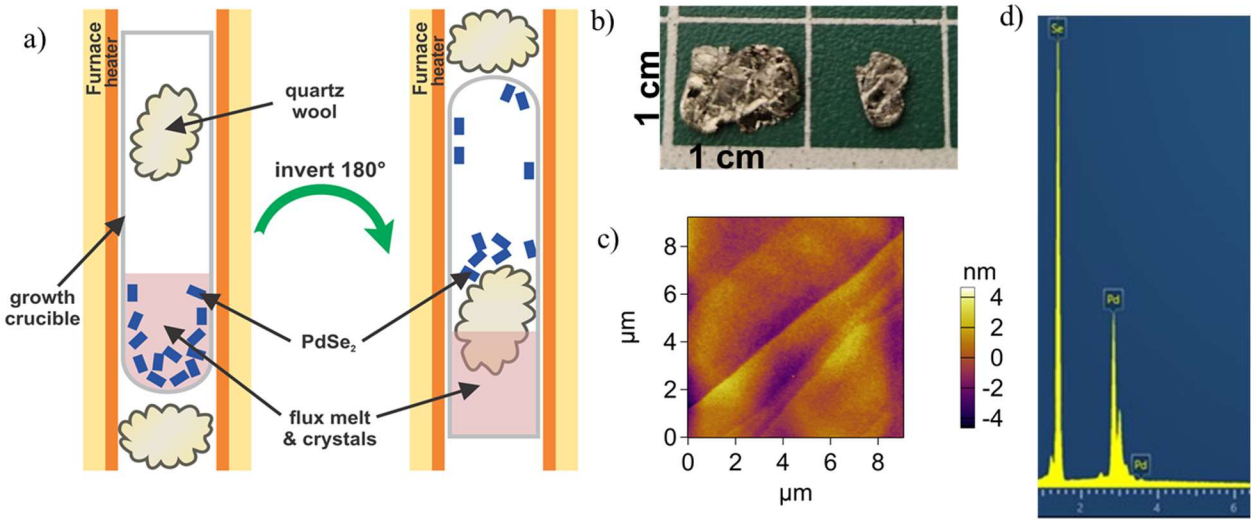

Figure 11 (a) Schematic diagram of the method for growing $PdSe_2$ crystals from a high-temperature solution; (b) photograph of $PdSe_2$ crystals; (c) AFM image of the crystal's layered structure; (d) EDS spectral analysis (atomic %), Pd/Se ratio: 1/1.9

Next a new ampule was prepared, filled with a ratio $PdSe_2$/Se = 1:7 and put in a furnace. The temperature was increased in a controlled manner at a rate of 20° C/h to 850 °C and maintained for 3 days to homogenize the solution. Then the temperature was lowered to 400° C at a rate of 1° C/h, and crystallization took place in this range. Final cooling to room temperature was performed at a rate of 40° C/h. The obtained $PdSe_2$ crystals were characterized by a well-defined structure (Fig. 11 b, c), suitable for applications in electronic and optoelectronic devices. Energy-dispersive elemental mapping showed a uniform distribution of Pd and Se, and the analysis of Fig. 11d showed an almost stoichiometric composition of $PdSe_2$.

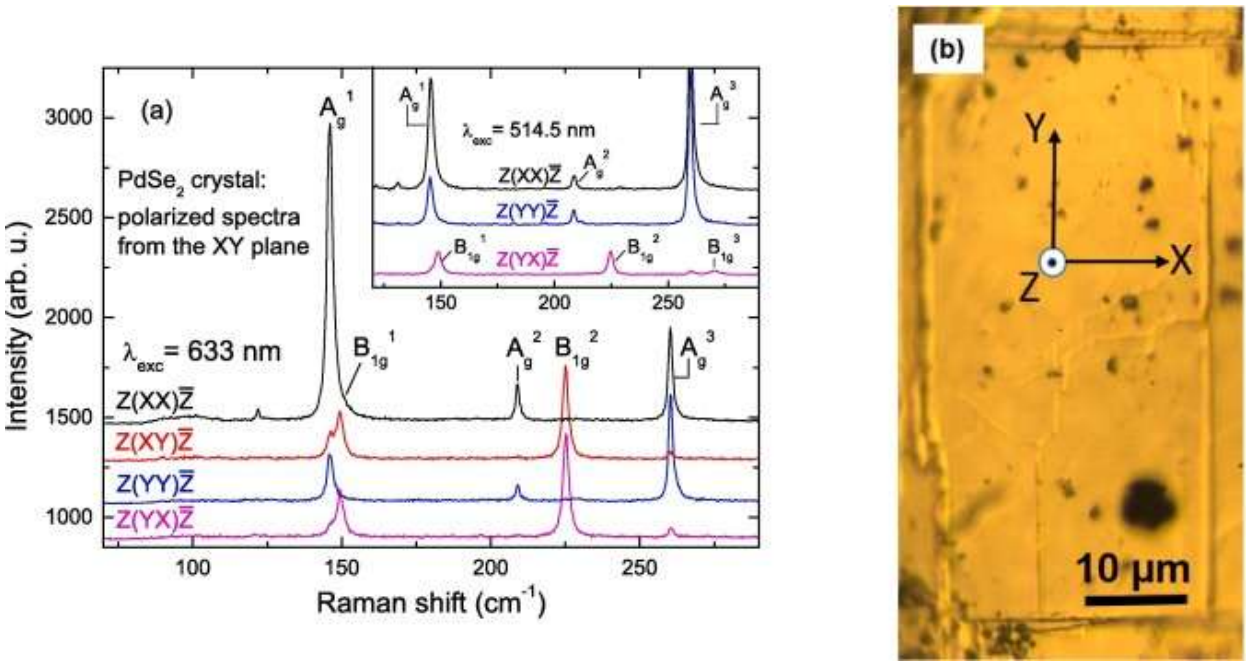

Figure 12 Raman spectroscopy of a $PdSe_2$ crystal: (a) polarized Raman spectra excited at 633 nm in geometric configurations denoted by Porto notations. Inserted figure: Same as the main panel for laser excitation at 514.5 nm; (b) optical microscope image of the studied single-crystal region with indication of the principal crystallographic directions used in the measurement configurations.

Fig. 12 b shows an optical microscope image of the investigated rectangular single crystal region, judging by the spectral quality. The crystallographic axes are determined by referring to literature data [8,9], reporting a maximum in the intensity of $A_g^{\ 1}$ (145 cm $^{-1}$) for Z (XX) $\bar{Z}$ geometry at an excitation wavelength of 532 nm. In the measurements, for both 633 nm and 514.5

nm excitation wavelengths, the intensity of A_g^1 shows a maximum in parallel polarization for an excitation beam polarized along the short side of the rectangle shown in Fig. 12b, and a minimum for polarization along its long side. Therefore, the short side of the rectangle should be approximately oriented along the *a axis* and the long side along the *b axis*, as depicted in Fig. 12b.

The full width at half-maximum (FWHM) of the frequency modes obtained from the spectra are summarized in Table 3. The linewidths (FWHM typically around 2 $cm^{-1)}$ indicate good crystalline quality of the samples. Only the B_{1g}^3 mode at 269.5 cm^{-1} has a linewidth more than twice as large and shows obvious resonant behavior, with measurable intensity only at 514.5 nm excitation wavelength. It has recently been found that the frequencies of the Raman modes in $PdSe_2$ show a significant hardening when going from bulk crystal to monolayer due to strong interlayer coupling and hybridization [8,10]. As expected for a bulk crystalline sample, the measured frequencies are closer to the lower limit of the values reported in the literature.

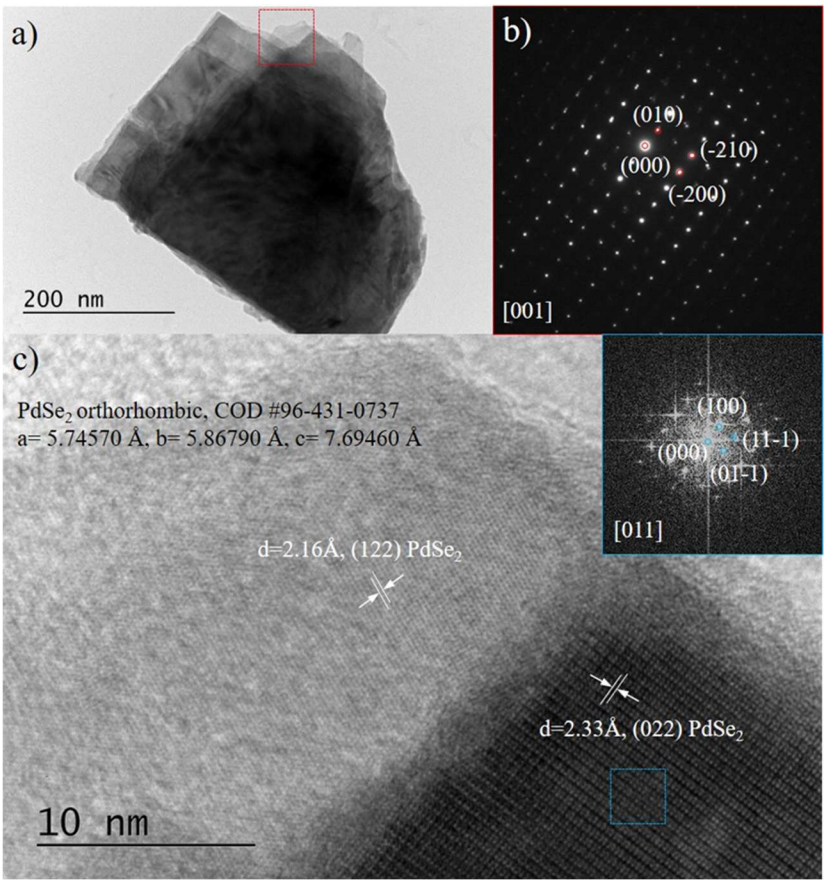

Figure 13 (a) Bright-field TEM image, (b) the corresponding SAED pattern, and (c) HRTEM image along with the Fast Fourier Transform of the blue square region (inset) of the $PdSe_2$ crystal

The morphology of the flake exfoliated from a single crystal of $PdSe_2$ by ultrasound is presented in Fig. 13a, where the presence of a layered structure is clearly visible [11]. The performed SAED analysis (Fig. 13b) is evidence of a single crystal structure of the crystal, which allows us to confirm the diffraction reflections using the open database. belonging to orthorhombic $PdSe_2$ and to determine its orientation along the zone axis [0 0 1] and unit cell parameters a = 5.74570 Å, b= 5.86790 Å and c = 7.69460 Å.

From the image taken in high-resolution mode (Fig. 13c) in the area surrounded by a red square in Fig. 13(a), the crystal planes (1 2 2) and (0 2 2) of $PdSe_2$ in two adjacent regions of the flake are visualized. Also from Fig. 13c) the interplanar distances of a family of planes (1 2 2) and (0 2 2) have been calculated.

II Applications

II.1 Applications of transparent, conductive $PtSe_2$ nanosheets as light shutters based on polymer-dispersed liquid crystals (PDLC)

The extremely high transparency of $PtSe_2$ in the near-infrared spectral range makes it an excellent material for reducing power consumption by modulating the transmission of near-infrared light. For example, in the design of smart windows that can selectively modulate the transmission of light and color. That is, the integration of $PtSe_2$ as a supporting transparent conductive layer in liquid crystal (LC)-based devices opens a new path for so-called ITO-free switches, displays, as well as a variety of optical devices operating in the near-infrared spectrum. In addition, $PtSe_2$ is stable in air, which brings additional advantages in the applications of the material in optoelectronics.

Liquid crystals (LC) are birefringent materials characterized by two refractive indices – ordinary n_0 and extraordinary n_e. Their ability to change their arrangement instantaneously under the influence of an electric field makes them ideal for controlling light, thanks to which they find wide application in modern technologies: in liquid crystal displays (LCD); for making optical elements such as lenses [12,13], half-wave plates, phase modulators, etc. [14,15], in photonics, biomedicine, 6G communications, and autonomous cars.

When liquid crystal molecules are mixed in a polymer matrix (isotropic material), they form composite materials, the so-called polymer-dispersed liquid crystals (PDLC). Polymer-dispersed liquid crystals are polymerized liquid crystal droplets with dimensions less than 1 micron [16]. embedded in a polymer matrix.

The operating principle of PDLC devices is based on the reorientation of liquid crystal molecules in the polymer matrix upon application of an electric field, which leads to controlling the optical response of the system by microscopic liquid crystal droplets, chaotically distributed in a polymer matrix. In its initial state, the PDLC structure scatters light due to the mismatch of refractive indices between the polymer medium (type NOA 65, refractive index $n_p = 1.524$) and the liquid crystal (type E7, with a ordinary $n_0 = 1.521$ and extraordinary $n_e = 1.72$ refractive index), forming a photocurable adhesive polymer matrix with a weight ratio of 3:7. When an external electric field is applied, the liquid crystal molecules are oriented in one direction, which allows the

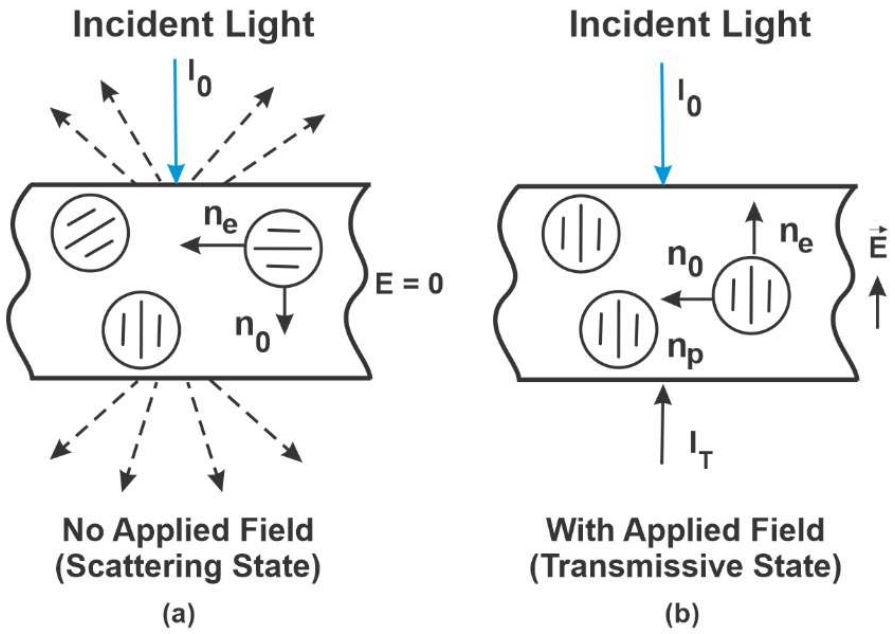

Figure 1. Principle of operation of PDLC: a) No electric field applied between the electrodes (off state) and b) an electric field applied between the electrodes (on state)

refractive index of the polymer medium (n_p) to be equalized with that of the liquid crystal (n_0). and control over the optical transmittance of the device. That is, PDLC devices work on the principle of light scattering and more specifically:

(i) In the absence of an applied electric field (opaque state ((OFF state)), the liquid crystal molecules in the droplets are oriented randomly. When light encounters the boundary between the polymer and the droplet, due to the difference in the coefficients n_o and n_p, it is refracted and scattered in all directions. The scattering of the incident light is due to the mismatch in the

refractive indices of the liquid crystal n_o and the polymer matrix n_p, which gives the device an opaque or matte appearance. [17] (Fig. 14a).

(ii) When an electric field is applied (transparent state) ((ON state)), the liquid crystal molecules are aligned in one direction (i.e., a collective reorientation of the liquid crystal molecules in a direction corresponding to the direction of the electric field occurs). In this orientation, their ordinary refractive index n_0 is chosen to coincide with that of the polymer matrix n_p. As a result, the mismatch in the refractive indices of the liquid crystal LC molecules and the polymer matrix is minimized, which significantly reduces light scattering and leads to the passage of light through the PDLC structure ($n_0 \sim n_p$, the light does not "see" a boundary between the polymer and the droplet, as a result of which it passes straight through without scattering) (fig.14 b).

Thus, by fine control of the applied electric field, it is possible to achieve continuously adjustable optical transmission, which allows precise tuning of the transmission depending on the specific requirements of the application. Overall, PDLC technology offers a versatile and innovative solution for dynamic light control, making it an essential component in modern smart glass applications. [18], as well as for making phase modulators [19], in holography [20] and display devices. [21]

In traditional applications, as transparent conductive layers, thin layers (~200 nm) of indium tin oxide (ITO) are most often used, which have high electrical conductivity, excellent optical transparency and chemical stability. Despite these advantages, the limitations in the availability of indium in nature and its environmental cost stimulate research into the development of alternative materials. Not least are the significantly low transmittance values of ITO in the infrared region of the spectrum. In this aspect, $PtSe_2$ is an excellent alternative to ITO, offering comparable or even better properties in the near infrared region (Fig. 15)

Spectrophotometric measurements were performed to determine the optical properties of $PtSe_2$, covering both the ultraviolet and near-infrared regions. Spectrophotometric analysis showed that the highest transmission values were observed in the infrared range, with an optimal thickness for maximum efficiency identified for a $PtSe_2$ layer with a thickness of 7 nm. This thickness provides a good balance between high electrical conductivity and stable transparency, making $PtSe_2$ an excellent candidate for applications in polymer-dispersed liquid crystal (PDLC) devices.

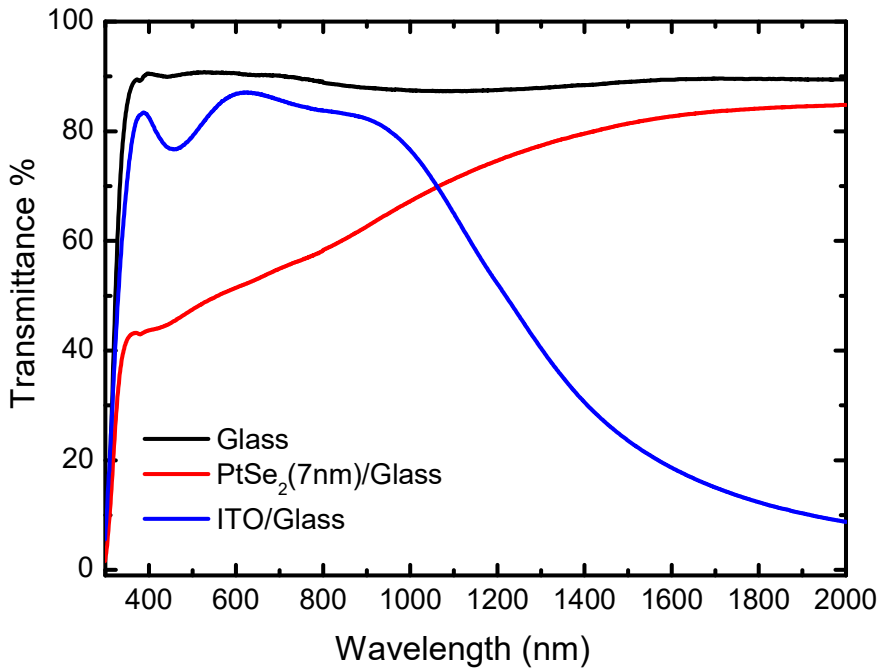

Figure 2. Optical transmission of $PtSe_2$ layer (7 nm)/glass in the near infrared spectral range (for comparison, the spectra of a commercial ITO layer/glass are also shown) in the range 320 nm - 2000 nm

The process of making PDLC devices using $PtSe_2$ nanolayers is shown in Fig. 16.

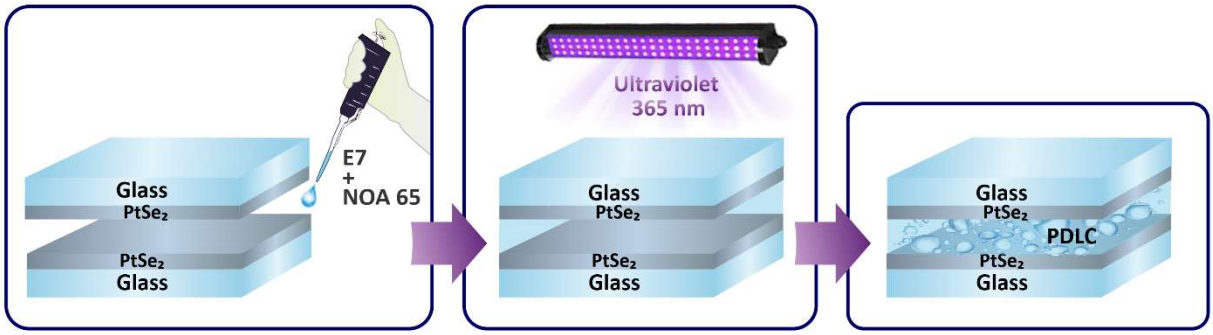

Figure 3 Making PDLC $PtSe_2$ - based devices.

To measure the electro-optic modulation and characteristics of PDLC structures based on $PtSe_2$ and ITO electrodes, an optical scheme was built, shown in Fig. 17. A Cobolt Rumba laser emitting at λ = 1064 nm was used as the irradiation source. Additionally, a He - Ne laser with a

wavelength of 633 nm was used to analyze the behavior of the structure under different illumination conditions. This experimental setup provided a reliable comparison of the optical and electrical properties of the different materials used in PDLC devices.

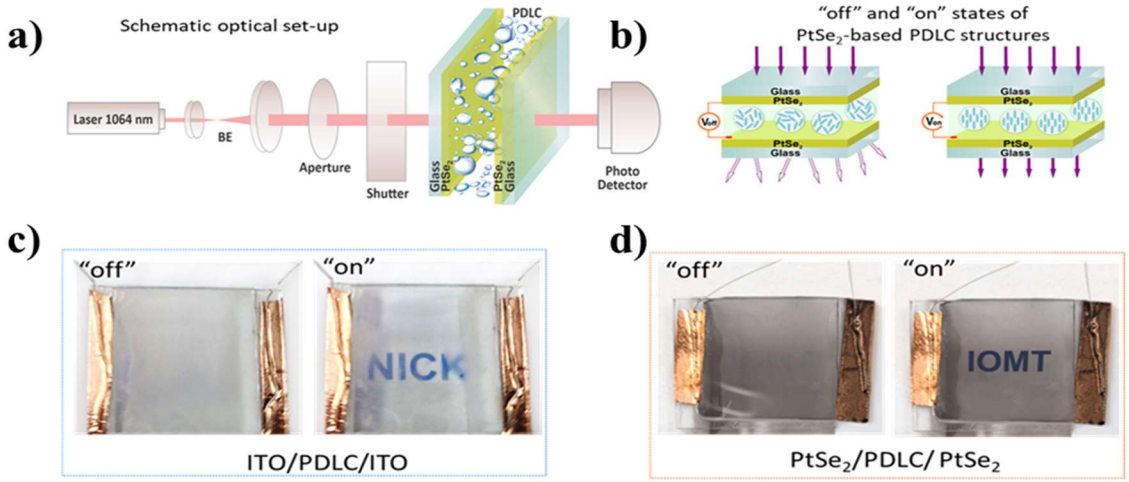

Figure 4. (a): Experimental setup for measuring electro-optical characteristics of PDLC structures and (b) illustration of the principle of operation, photos of PDLC structures based on (c) ITO and (d) $PtSe_2$ electrodes in "off" and "on" states

Figure 17b illustrates the operation of a PDLC made with $PtSe_2$ electrodes. Real PDLCs based on ITO and $PtSe_2$ in the "off " and " on " states are shown in Fig. 17c and Fig. 17d. As can be seen, the device made of ITO is more transparent than the device made of $PtSe_2$. This result is expected and corresponds to the data for optical transmittance in the visible region of both materials presented in Fig. 15.

In Fig. 18 The results of the comparative analysis of the transmission between PDLC structures made of $PtSe_2$ and ITO as a function of the applied voltage under 633 nm and 1064 nm laser illumination are shown. To perform a quantitative analysis of the device performance, two key quantities are used: threshold voltage (V_{th}) and saturation voltage (V_{sat}). V_{th} determines the minimum voltage required to reach 10% of the maximum transmittance, while V_{sat} corresponds to the voltage at which 90% of the maximum transmittance is reached [22] . These parameters play an essential role in understanding the dynamics of light modulation in the structure, which is

crucial for the practical applications of PDLC devices. They also reflect the electro-optical performance of the devices and their potential applicability in industry.

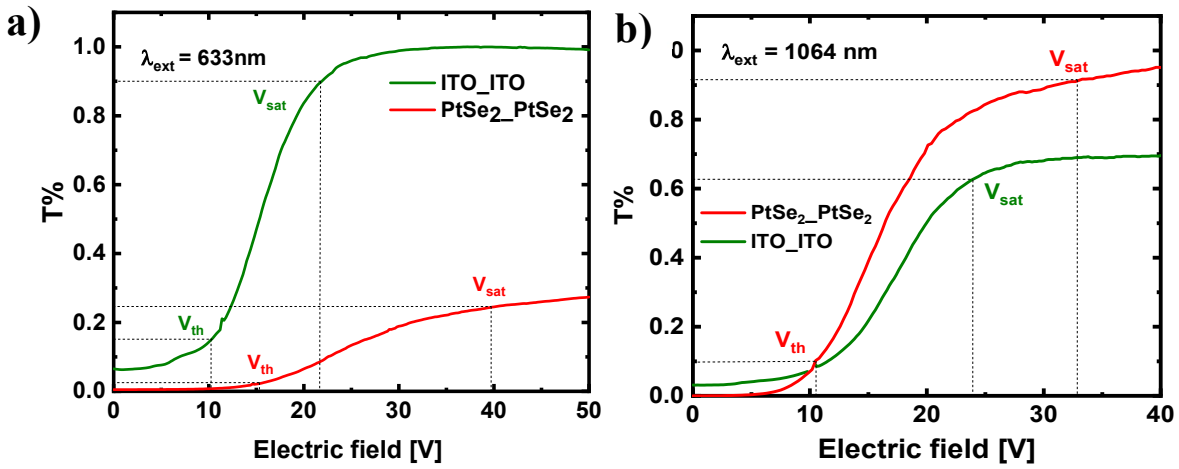

Figure 5. Dependence of optical transmittance on applied voltage of PDLC devices based on $PtSe_2$ and ITO electrodes upon irradiation with a) 633nm and b) 1064 nm laser radiation.

For the device fabricated on the basis of $PtSe_2$and illuminated with 1064 nm, values V_{th} ($PtSe_2$) ~ 9V and V_{sat} ($PtSe_2$) ~ 25.6V are obtained. On the other hand, for the device fabricated on the basis of ITO, values V_{th} (ITO) ~ 11V and V_{sat} (ITO) ~ 24V were measured upon irradiation with 1064 nm Table 1.

Table 1 Operating voltages of PDLC light switch fabricated based on ITO and $PtSe_2$ conductive layers.

Device	V_{th} [V]	V_{hour} [V]	Response time [ms]
ITO_ITO	11	24	3-50
Pt Se_2 _Pt Se_2	9	25.6	40

As can be seen from Fig. 18, both devices have similar saturation voltages, but the $PtSe_2$-based PDLC structure has a lower threshold voltage compared to the one made entirely of ITO. This suggests a higher sensitivity and improved efficiency of the $PtSe_2$ structure in the infrared

spectral range. In addition, the response and relaxation times of the $PtSe_2$-based PDLC structure are 40 and 62 ms, which further confirms its efficiency.

Conclusion: It has been demonstrated that the intensity of the transmitted infrared light can be controlled by an applied external voltage and a PDLC structure based on $PtSe_2$ can function as a light shutter for the near infrared region. Furthermore, $PtSe_2$ can replace the commonly used ITO conductive layers not only because of the limited sensitivity of ITO in the near infrared spectral range, but also because of other practical advantages. This study highlights the importance of $PtSe_2$not only as an alternative to ITO, but also as a material with the potential to significantly improve the functionality and efficiency of future optoelectronic technologies.

II.2 Application of $PdSe_2$ in a field effect transistor (FET)

To explore potential future applications of $PdSe_2$, an idea for a field effect transistor has been created by transferring a flake from the crystal onto previously deposited electrodes Fig. 19. With additional processing, the conductivity of $PdSe_2$ can be easily changed to electronic (vacuum annealing) or hole (molecular doping with F_4-TCNQ) [23] .

For the fabrication of $PdSe_2$ -based field effect transistors (FET), the first step is the transfer of mechanically exfoliated $PdSe_2$ flakes from the bulk crystal onto a previously prepared substrate suitable for electrical measurements. The device is fabricated on a Pt test chip (https :// www. ossila. com /) and is an n -type doped silicon chip with thermally grown SiO_2 (300 nm), which also acts as the Gate. The metal electrodes for Source and Drain are predefined and represent a 50 nm coating Pt and 10 nm adhesion T i layer at a distance of 10 μ m and a width of 4 μ m (Fig. 20b).

The deterministic transfer process includes: exfoliation of thin flakes from a bulk crystal of $PdSe_2$with adhesive tape (Nito tape). After sufficient thinning, the flakes are transferred onto PDMS by gluing. Under a microscope, a suitable flake is selected and aligned and positioned relative to the substrate contacts. After alignment, the $PdSe_2$/PDMS structure is glued to the substrate and heated to ~190 °C to achieve good adhesion. Finally, the polymer layer is slowly peeled off, so that the $PdSe_2$ the scale remains precisely positioned on the device – Fig. 19. The made device is shown in Fig. 20 a, c

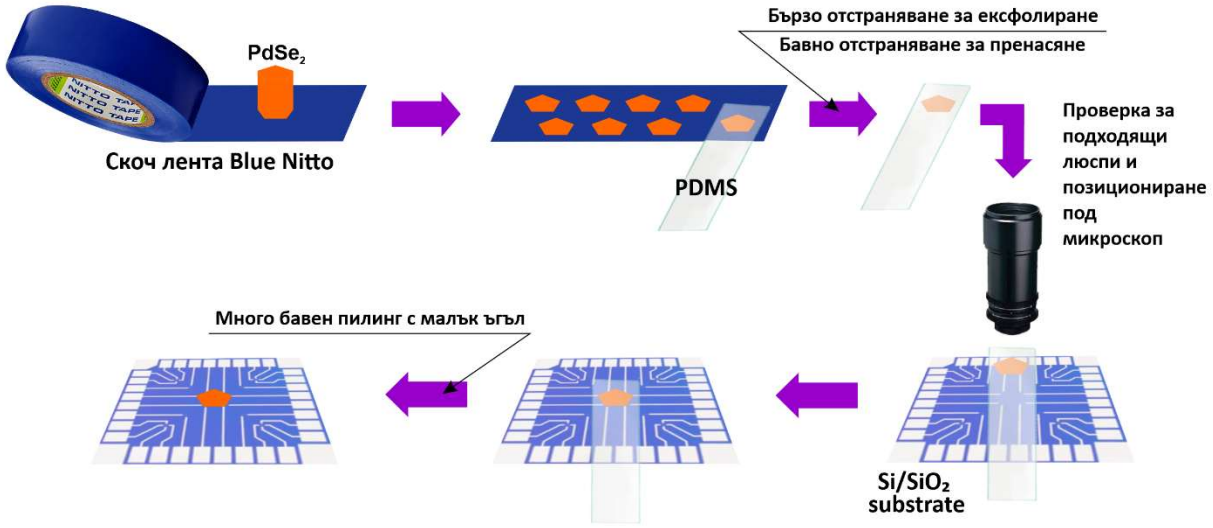

Figure 6. Fabrication of a transistor from $PdSe_2$.

After the transistor was made, its electrical characteristics were also studied. First, the so-called 2D conductivity was checked σ, which is given by the following equation:

$$\sigma = \frac{I_{ds}}{\Delta V}\frac{L}{W} \tag{5}$$

where I_{ds} is the current flowing between the emitter and the collector, ΔV is the voltage drop, and L/W is the length/width ratio of the channel. When applied (room temperature), a voltage of +80 V to the base, the conductivity reaches 4.11 x 10^{-4} S (Fig. 20d). Similar values have been observed in devices made of thin (11 nm) $PtSe_2$ layers (1× 10^{-4} S) [24] . This value is several orders of magnitude higher than other semiconductors. TMDCs such as MoS_2 [24] . It should be emphasized that this difference is for measurements made at room temperature. Also, advances in synthesis technologies and process optimization for the fabrication of NTMDs FET (improvement of contact between electrodes and $PdSe_2$, minimization of defects, optimization of the working channel, etc.) would lead to even greater conductivity. The device thus fabricated demonstrates current

modulation of the order of of 10^3. This high modulation makes $PdSe_2$ a promising candidate for an active element in transistor fabrication.

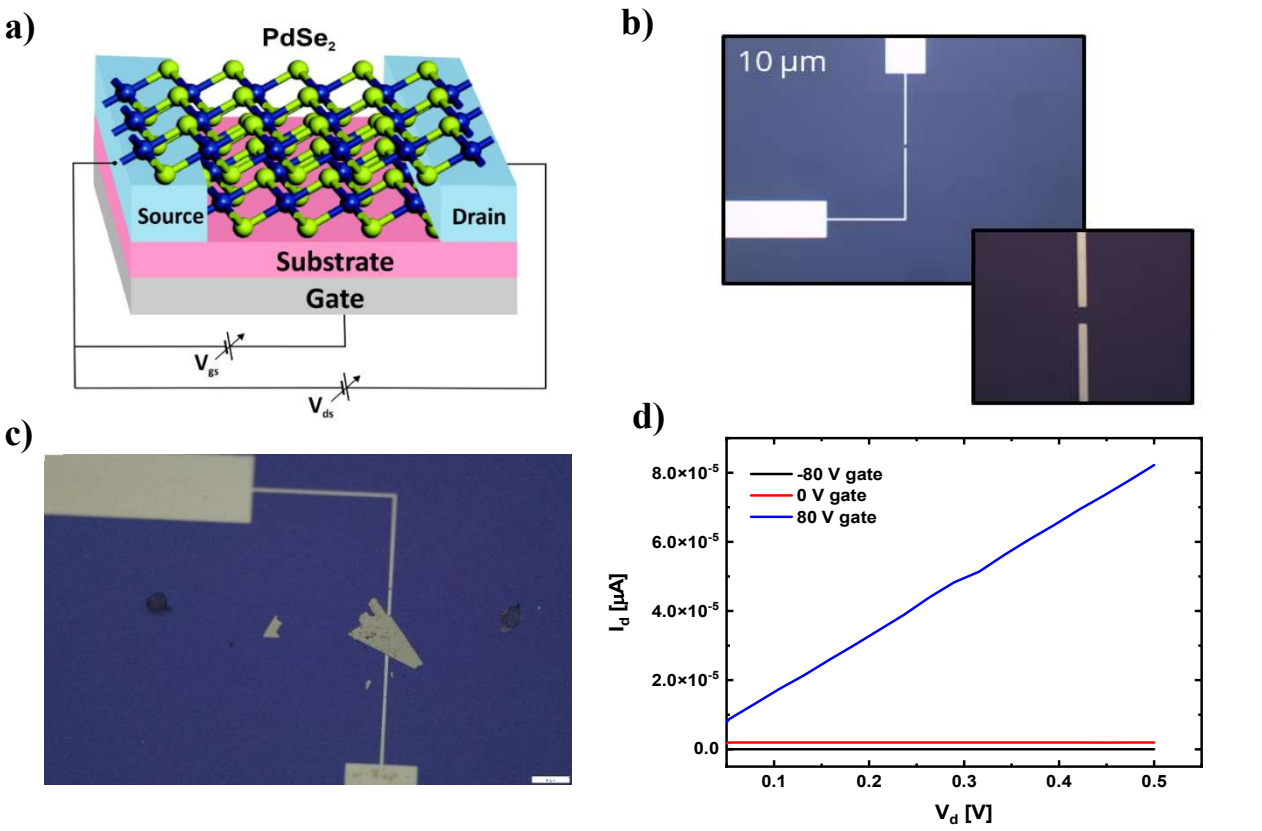

Figure 7. a) Schematic of a $PdSe_2$ field effect transistor. b) Optical microscope photograph of electrodes for FET fabrication. c) Optical microscope images of a field effect transistor fabricated from transferred $PdSe_2$ at 20x magnification marker 20 µm. d) Operating characteristic of $PdSe_2$ FET.

In addition, the developed device is light-responsive. The behavior of the transistor under illumination with light of wavelength 405 nm (violet light) was investigated (Fig. 21). This shows that the $PdSe_2$ transistor has potential for application as a photodetector or phototransistor.

Figure 8) Behavior of the $PdSe_2$ device under 405 nm illumination light, b) the region enclosed by the red square in (a).

II.3 $PtSe_2$ as antibacterial coatings against *Escherichia* coli

In recent years, medical technology has made extraordinary progress, which has also contributed to more effective control of bacterial and viral infections. However, public health and the prevention of the spread of pathogens remain among the main priorities for both European health institutions and international organizations supporting less developed regions. An additional problem is the increasing antibiotic resistance, which is on the way to becoming a serious threat to public health. Many pathogenic microorganisms are developing resistance to traditional antimicrobial agents, which requires urgent measures to find innovative control and treatment strategies. The development of innovative approaches to tackle infectious diseases, including new antimicrobial therapies, vaccines and resistance control strategies, will play a key role in the future of public health and population security on a global scale.

In general, internationally recognized ISO standards developed by the International Organization for Standardization (ISO) are used to test the antibacterial activity of various materials. In the context of photocatalytic materials, ISO 27447:2019(E) is an important standard for testing the antibacterial activity of ceramic coatings, as well as materials containing photocatalysts. This standard was used to conduct the present study. study on $PtSe_2$ nanolayers, with antibacterial activity evaluated in the dark and under ultraviolet (UV) irradiation.

Typically, photocatalysts exhibit a wide range of beneficial properties when exposed to light, including degradation of air and water pollutants, self-cleaning, fouling prevention, and

antibacterial activity. These effects result from the generation of highly reactive oxygen species, such as superoxide (O_2^-) [25] , hydroxide radical ($OH\cdot$), and singlet oxygen ($^1O_2$), which interact with organic molecules on the surface of the material [26,27]. Of particular interest is the energy-efficient nature of photocatalytic processes, especially when the photocatalytic action is driven by sunlight or low-energy artificial lighting.

The method that was used to study the antibacterial activity of photocatalytic materials involves preparing a bacterial suspension and contacting the bacterial suspension with the surface of the test sample under ultraviolet light.

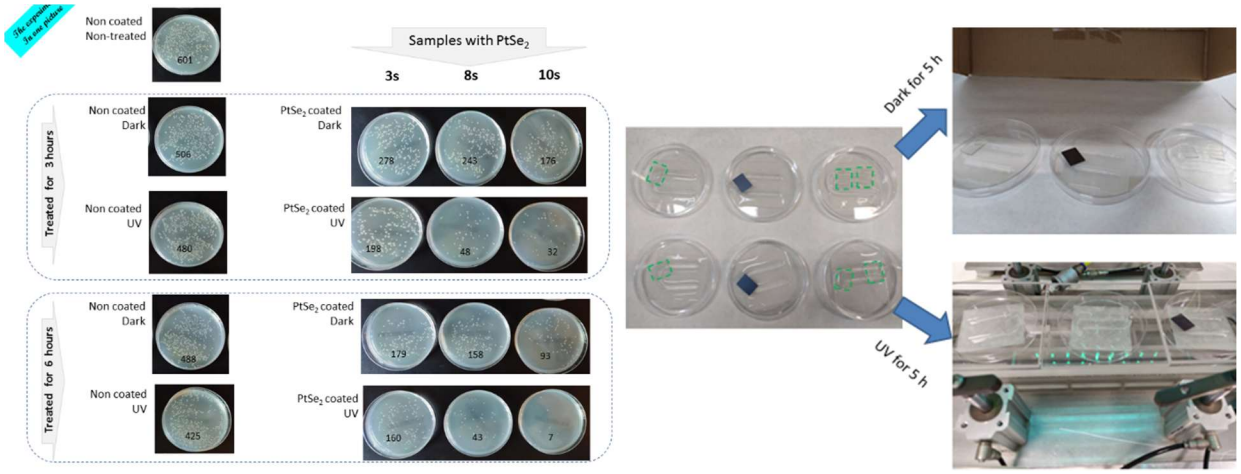

Figure 9a study on the antibacterial activity of $PtSe_2$ nanolayers.

The procedure consists of applying the bacterial suspension to the surface of the sample (a nanolayer of $PtSe_2$ deposited on glass) placed in a Petri dish. The concentration of bacteria was determined using a UV-VIS spectrophotometer, assuming that an absorbance of 0.001 at a wavelength of 600 nm corresponds to approximately 10^6 colony-forming units per milliliter (CFU/mL). Based on this relationship, the concentration of the bacterial suspension was recalculated to 2×10^6 CFU/mL to ensure optimal conditions for the experiment.

The samples are then placed in 80 mm diameter petri dishes, as required by the ISO standard. On each dish, filter paper, a U-shaped glass plate, 4 mL of deionized water, the test sample, 50 µL of the bacterial suspension, a transparent protective layer, and finally a glass cover

for samples examined in the dark, or a quartz cover for those exposed to UV radiation, are sequentially added (Fig. 22).

prepared, including both an uncoated control glass and the test material $PtSe_2$. The above steps are repeated for three different thicknesses of 7 nm, 9 nm and 12 nm of the resulting $PtSe_2$nanolayers. The samples are processed in complete darkness or exposed to UV radiation with an intensity of 0.1 W/m² for a period of 6 hours.

After treatment, the bacterial colonies surviving on the surface of the samples are collected by washing with saline. Then, 100μ l of each solution is dropped onto a special nutrient agar, providing conditions for bacterial growth.

The dishes are then placed in an incubator at 37°C for 24 hours to allow the surviving bacteria to form colonies. The resulting colonies are individual white dots that can be counted and compared (Fig. 23). The number of colonies formed serves as the main indicator of antibacterial effectiveness – the fewer the colonies, the higher the activity of the tested material.

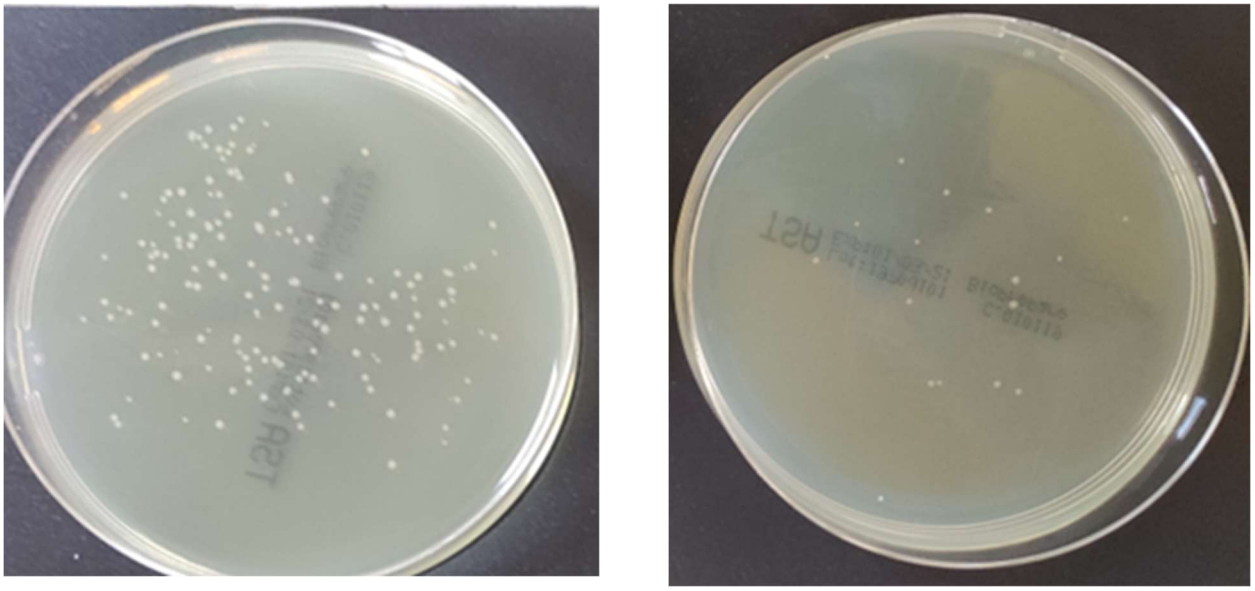

Фигура 10. Photos of petri dishes containing agar medium with colonies of surviving bacteria.

The test results are presented through images, as well as through a quantitative comparison of the number of colonies in the different experimental conditions: control substrates, treated in the dark, and under the influence of UV light.

During the study, two mechanisms of antibacterial action were identified: (i) without light irradiation, typical of 2D materials, and (ii) upon light irradiation, typical of semiconductors (influence of photocatalytic effect).

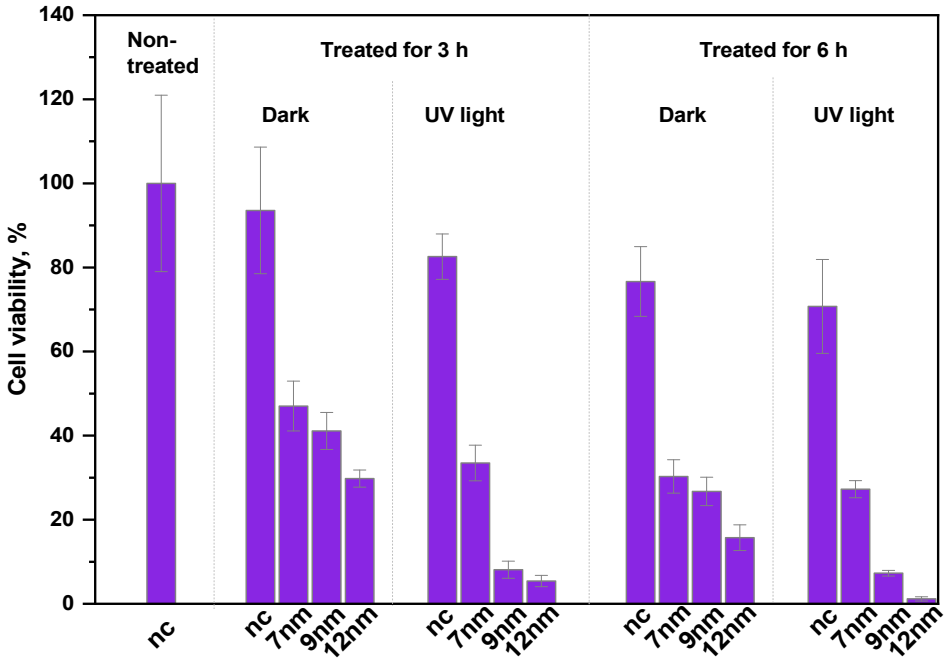

Figure 11 Antibacterial effect of $PtSe_2$ layers with different thicknesses depending on the time spent in the dark and light (3 hours and 6 hours).

When the samples are in the dark, the antibacterial activity of the $PtSe_2$ coatings increases gradually with increasing Pt deposition time. layer. After 3 hours of treatment (Fig. 24), cell viability varied between ~47% $PtSe_2$ -7nm and ~30% $PtSe_2$ -12nm, while after 6 hours of treatment (Fig. 24), the viability decreases to values between ~30% ($PtSe_2$ 7nm) and ~15% $PtSe_2$ -12nm. This can be explained by the increased surface roughness and higher coverage of the thicker samples – PtSe2 (7 nm), $PtSe_2$ (9 nm) and $PtSe_2$ (12 nm), which facilitates the mechanical destruction of bacteria [28] . In addition, the surface energy of these coatings can contribute to a stronger interaction between bacterial cells and the material, which further enhances the antibacterial effect. It is important to emphasize that this mechanism of action is relevant for the development of new antimicrobial surfaces in medicine, such as for the development of sterile

instruments and water filters. Similar observations have been reported for other two-dimensional materials, such as molybdenum disulfide (MoS_2) [29] and tungsten diselenide (WSe_2) [30] , indicating that this class of materials has significant potential for the development of new antibacterial coatings.

When treated with ultraviolet light, the three studied $PtSe_2$ coatings exhibit different behavior (Fig. 24). The $PtSe_2$ (7 nm) coating shows low sensitivity to light, as the cell viability in the dark and under UV irradiation remains similar – ~47% and ~33% for the samples treated for 3 hours, and ~31% and ~27% for those treated for 6 hours. On the other hand, the $PtSe_2$- 9 nm and $PtSe_2$- 12 nm coatings demonstrate significantly increased antibacterial activity under light, indicating a photoinduced antibacterial behavior that becomes more noticeable with increasing Pt layer deposition time. Specifically, the cell viability of $PtSe_2$ (9 nm) after 6 hours of irradiation decreases to 7.3%, while for $PtSe_2$- 12 nm it reaches 1.2%. This means that the material could be used to create self-disinfecting surfaces, which would be particularly useful in hospital settings.

The high photoinduced antibacterial activity of $PtSe_2$ (12 nm) may be due to several factors: (i) high crystallinity; (ii) the presence of a band gap of ~0.64 eV, allowing electron excitation upon light irradiation; (iii) a Se-deficient surface, which favors the generation and trapping of excited electrons. It is assumed that the created charge carriers contribute to the formation of oxygen radicals (ROS), which destroy bacteria through oxidative stress. To verify this hypothesis, measurements were made using an Electron Paramagnetic Resonance (EPR) analysis. This technique allows the detection of surface-generated oxygen radicals upon UV irradiation of $PtSe_2$ coatings. For this purpose, an experimental approach was used, based on the capture and identification of short-lived ROS by highly sensitive spin traps. Specifically, a nitron DMPO (5,5-dimethyl-1-pyrroline N-oxide) spin trap was used, which is well known for its ability to form stable paramagnetic adducts with a number of radicals, including hydroxyl (·OH) and superoxide radicals (O_2). DMPO itself is “transparent” for EPR (does not exhibit its own electronic paramagnetic resonance signal), but upon interaction with ROS it participates in electron transfer leading to the formation of nitroxide spin adducts. These adducts, due to their paramagnetic nature, can be easily detected by EPR spectroscopy, which allows for both qualitative and quantitative analyses of the oxygen radicals present.

Fig. 25 illustrates the spectral characteristics of adducts obtained during the interaction between ROS and DMPO under UV irradiation of $PtSe_2$ with different thicknesses: (7 nm), (9 nm) and (12 nm). The control spectrum (a), recorded in the dark, does not show a signal from oxygen radicals, which confirms the absence of photogenerated ROS. In contrast, spectra (b), (c) and (d), recorded after UV irradiation, clearly demonstrate the presence of characteristic signals associated with the formation of radicals. The dominant signal, marked with asterisks, belongs to the DMPO/·OH complex, whose EPR characteristics include four distinct lines with an intensity ratio of 1:2:2:1 and hyperfine coupling constants $a_N = a_H = 14.9$ Gauss [31] , in full agreement with the literature.

In addition to the main signal, additional components characterized by hyperfine constants $a_N = 14.7$ Gauss, indicated by solid circles, are observed in spectrum (c). These signals probably reflect the presence of degraded forms of DMPO resulting from side reactions. The additional set of lines in the same spectrum points to the possible presence of an alkyl radical, which most likely represents an oxidation product of DMPO. This hypothesis is supported by simulations of the spectral parameters, showing good agreement with the values $a_N \approx 15.5$ Gauss, $a_{H1} \approx 25.8$ Gauss and $a_{H2} \approx 1.7$ Gauss presented in spectrum (c'). Although the DMPO/·OH adduct is predominant in the spectra, the possibility that it originates from the transformation of the unstable DMPO/·O_2^- complex cannot be excluded. This superoxide adduct is known to have a limited lifetime in aqueous media, with its degradation time being strongly dependent on the acidity of the medium: $t_{1/2} = 27$s at pH=5 and $t_{1/2} = 91$s at pH=9. This rapid degradation leads to the formation of DMPO/·OH as a by-product [32]

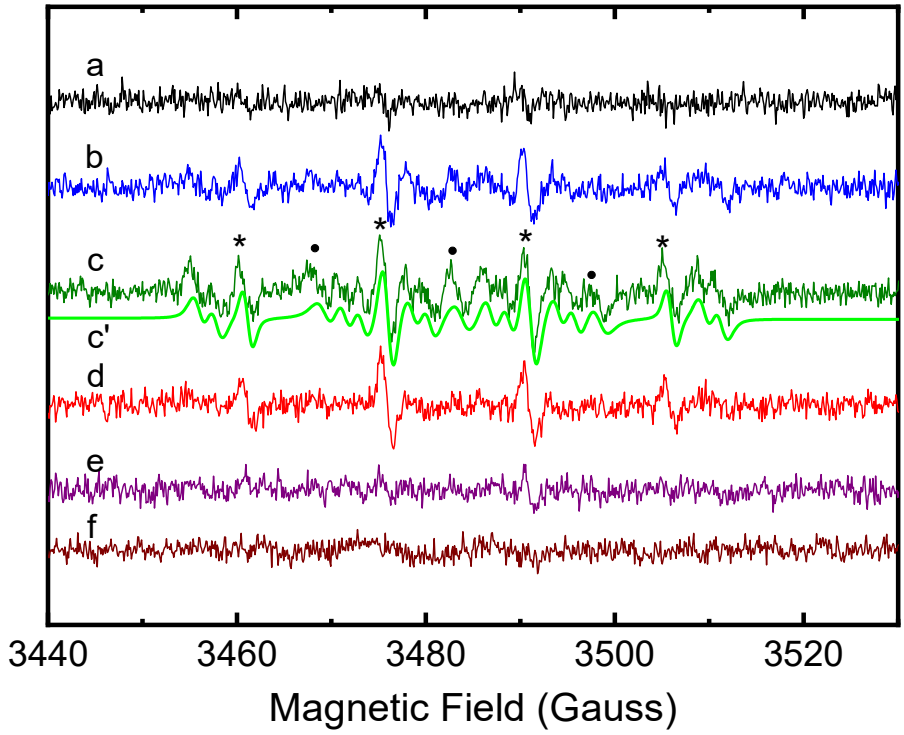

Figure 12EPR spectra: a) of sample ($PtSe_2$ 12 nm) before illumination; b), c) and d) of samples ($PtSe_2$ 7 nm), ($PtSe_2$ 9 nm) and ($PtSe_2$ 12 nm) after 1.5 min. illumination; c') is a theoretical fit to the experimental spectrum c); e) is the spectrum of ($PtSe_2$ 12 nm) obtained in the presence of 20% (v/v) DMSO; (f) is the spectrum of (Pt 10s) obtained when the DMPO spin trap is dissolved in acetonitrile.

To test this hypothesis, the experiments were repeated in the presence of a 20% volume solution of dimethyl sulfoxide (DMSO), an organic solvent that is an effective scavenger of hydroxyl radicals but does not prevent the formation of superoxide adducts with DMPO. The resulting spectrum (e) shows a significant decrease in the intensity of the DMPO/·OH signal, which strongly indicates that the observed·OH radical does not originate from DMPO/O_2^-, but is formed directly by photoinduced oxidation of water by photogenerated holes (h^+) on the surface of the photocatalytic material.

In order to further confirm the ability of $PtSe_2$ to initiate electron transfer to molecular oxygen without the participation of the aqueous medium and the formation of OH radicals, an

additional experiment was carried out with acetonitrile. This organic solvent has a significantly higher solubility of oxygen and does not contain water, thus eliminating the possibility of secondary formation of hydroxyl radicals. In this environment, stabilization of the DMPO/$\cdot O_2^-$ adduct is expected. The obtained spectrum (f), however, did not show the presence of EPR active species, which once again confirms that upon UV irradiation of $PtSe_2$ in an aqueous medium the main mechanism for the formation of DMPO/·OH adducts is the direct oxidation reaction with the participation of photogenerated holes, and not through an intermediate superoxide step. This observation emphasizes the importance of the aqueous medium for realizing the full photocatalytic potential of $PtSe_2$ under UV exposure and opens prospects for its application in oxidation processes and water purification by generating highly reactive oxygen radicals.

This mechanism is similar to that of other semiconductor materials such as TiO2. [33] , but offers additional advantages, such as higher efficiency at lower energy levels.

It is important to note that the viability of bacteria on an uncoated glass substrate also decreased after treatment for 3 and 6 hours, but within the permissible limits according to ISO methods. In addition, Pt is a well-known catalyst [34] which raises the question of whether it is responsible for the observed antibacterial activity. However, XRD and XPS analyses did not reveal the presence of metallic Pt, allowing this hypothesis to be ruled out. This supports the conclusion that it is the structural and optical properties of $PtSe_2$ that are responsible for the reported antibacterial properties.

The presented results clearly show that $PtSe_2$ exhibits antibacterial activity against *Escherichia coli* both in the dark and under light irradiation. Compared with other known antibacterial materials, such as graphene oxide and TiO_2, $PtSe_2$ exhibits a combination of mechanical and photocatalytic effects, which may make it competitive in specific applications. These results can be related to the layered 2D morphology, crystal structure and optical properties of the prepared nanolayers. Further studies can focus on modifying the structure of $PtSe_2$ in order to further improve its antibacterial efficiency and expand its potential applications in industry and medicine.

The antibacterial photocatalytic activity of $PtSe_2$ coatings. and paves the way for their further research such as functional coatings for implementation in medical equipment, self-sterilizing surfaces, etc.

Conclusions:

An alternative to conventional transparent, conductive ITO electrodes: It has been demonstrated that $PtSe_2$ nanolayers can successfully replace indium tin oxide (ITO) as transparent, conductive electrodes in polymer-dispersed liquid crystal (PDLC) devices. Furthermore, it has been shown for the first time that $PtSe_2$ layers with a thickness of 7 nm operate effectively as light shutters in the near-infrared region (1064 nm).

$PdSe_2$ as an active element in field-effect transistors (FETs): The integration of $PdSe_2$ as an active channel material has been successfully achieved. The device was fabricated via the precise positioning (so-called "dry" transfer) of a $PdSe_2$ flake onto electrodes, exhibiting good electrical conductivity, light sensitivity, and high stability in ambient air.

Antibacterial activity of $PtSe_2$ layers against *Escherichia coli*: The antibacterial effectiveness of these layers has been confirmed. It was found that upon UV irradiation, bacterial viability is reduced to 1.2% due to the photocatalytic generation of reactive oxygen species (ROS).

Conclusion

This dissertation represents a comprehensive study aimed at developing technological methods for the synthesis and characterization of new 2D materials from the group of transition metal dichalcogenides (TMDCs) – specifically platinum diselenide ($PtSe_2$), platinum ditelluride ($PtTe_2$) and palladium diselenide ($PdSe_2$) and demonstrating their applications in optoelectronics and biotechnology. Several significant results were achieved in the course of the work:

The thermally assisted conversion (TAC) method has been successfully optimized to obtain nanoscale layers with controlled thickness. This approach has proven to be an efficient and scalable alternative to traditional chemical vapor deposition (CVD), allowing synthesis on a variety of substrates at lower temperatures and atmospheric pressure. The proposed preparation techniques and developed recipes provide an innovative perspective for the synthesis of $PtSe_2$ by the TAC approach, which allows uniform coverage over large areas and the use of inexpensive substrates (e.g. glass). Compared to conventional methods, the TAC technology provides lower processing temperatures, better control over the layer morphology, and scalability potential. In addition, the possibility of integration with various substrates makes this method promising for the development of optoelectronic systems, including infrared switches, energy-efficient devices, and smart photonic structures.

Through detailed analysis of the structural, morphological and optical properties, a close relationship between the synthesis conditions and the physical characteristics of the materials was established. It was proven that the layers retain their stability and high crystallinity, which is critical for their practical application.

$PtSe_2$ as a transparent conductive material in liquid crystal devices (PDLC) was demonstrated, offering competitive characteristics compared to standard ITO, especially in the infrared region.

In the fields of biomedicine and nanotechnology, a strong light-activated antibacterial effect of $PtSe_2$ layers has been demonstrated, paving the way for the development of new types of self-disinfecting surfaces and sensors.

In conclusion, the obtained results confirm that noble metal dichalcogenides possess a unique combination of properties that make them extremely promising for the next generation of smart materials. The developed synthesis and transfer methods provide a solid basis for future research aimed at integrating these 2D structures into flexible electronics, highly sensitive photodetectors and catalytic systems. The work contributes to enriching the knowledge in the field of condensed matter physics and materials science by offering practical solutions to current technological challenges.

Main contributions of the dissertation

- Two different synthesis methods were investigated: (1) a two-step thermally activated conversion (TAC) process with a magnetron sputtered metal layer and a liquid precursor at atmospheric pressure and (2) low-pressure chemical vapor deposition (CVD) using solid precursors, on the structure and properties of 2D nanolayers of noble transition metal chalcogenides.
- Recipes have been developed for the controllable, reproducible synthesis of $PtSe_2$ and $PtTe_2$ on soda-lime glass, Si/SiO_2 and quartz by selenization of previously deposited Pt layers at atmospheric pressure and low temperatures.
- Single crystals of $PdSe_2$ have been successfully synthesized using the high-temperature solution method (flux method).
- The application of $PdSe_2$ as an active element in a field-effect transistor (FET) with pronounced photosensitivity has been demonstrated.
- For the first time was demonstrated the application of $PtSe_2$ -7 nm as transparent, conducting layers in polymer-dispersed liquid crystal structures operating as light switches in the near infrared region has been demonstrated.
- Antibacterial activity of $PtSe_2$ coatings against Escherichia coli has been demonstrated for the first time.

List of Publications by the Author Related to the Dissertation

1. N. Minev, K. Buchkov, N. Todorova, R. Todorov, V. Videva, M. Stefanova, P. Rafailov, D. Karashanova, Hr. Dikov, C. Trapalis, SH Lin, D. Dimitrov and V. Marinova "Atmospheric pressure TAC synthesis of 2D $PtSe_2$ layers and their integration in near infrared light shutters" *ACS Omega* 2024, 9, 14874−14886 (2024) https://doi.org/10.1021/acsomega.3c08235

2. Vera Marinova, Nikolay Minev, Blagovest Napoleonov, Daniela Karashanova, Peter Rafailov, Daniela Kovacheva, Velichka Strijkova, Bogdan Ranguelov, Valentina Mussi, Walter Fuscaldo, Dimitrios C. Zografopoulos, and Dimitre Dimitrov "$PdSe_2$ Single Crystals Synthesized by the Self-Flux Method" *Journal of Crystal Growth* 643, 127812, (2024) https://doi.org/10.1016/j.jcrysgro.2024.127812

3. Nadia Todorova, Nikolay Minev, Vera Marinova, Krastyo Buchkov, Vladimira Videva, Rosen Todorov, Peter Rafailov, Velichka Strijkova, Vassilis Psycharis, Tatiana Giannakopoulou, Ilias Papailias, Dimitre Dimitrov, and Christos Trapalis "Two-dimensional $PtSe_2$ coatings with antibacterial activity" *Appl Surface Sci*, 611, Part A, 155534 (2023) https://doi.org/10.1016/j.apsusc.2022.155534

4. Nikolay Minev, Irnik Dionisiev, Krastyo Buchkov, Hristosko Dikov, Vladimira Videva, Velichka Strijkova, Peter Rafailov, Dimitre Dimitrov and Vera Marinova "2D $PtTe_2$ Layers Synthesized by Thermally Assisted Conversion Method" XXXI International Scientific Conference ELECTRONICS – ET 2022, IEEE Xplore (2022) DOI: 10.1109/ET55967.2022.9920318

List of noticed independent citations

Nadia Todorova, Nikolay Minev, Vera Marinova, Krastyo Buchkov, Vladimira Videva, Rosen Todorov, Peter Rafailov, Velichka Strijkova, Vassilis Psycharis, Tatiana Giannakopoulou, Ilias Papailias, Dimitre Dimitrov, and Christos Trapalis "Two-dimensional $PtSe_2$ coatings with antibacterial activity" Appl Surface Sci, 611, Part A, 155534 (2023) https://doi.org/10.1016/j.apsusc.2022.155534

1. Zhen-Long Dou, Li Cheng, Zhi-Yong Wu, Li-Jiong Chen, Li Zhou, Qu-Quan Wang "Asymmetric Overgrowth of Au/AuPt/$PtSe_2$ and Au/AgPtSe_2 Heterorods for Optimizing Nonlinear Enhancements", Advanced Optical Materials, Volume12, Issue7, 2302140 (2024) https://doi.org/10.1002/adom.202302140
2. Francesca Ubaldi, Federica Valeriani, Veronica Volpini, Giusy Lofrano and Vincenzo Romano Spica "Antimicrobial Activity of Photocatalytic Coatings on Surfaces: A Systematic Review and Meta-Analysis" Coatings, 14(1), 92 (2024)
3. Lina Zhang, Kai Feng, Yizhe Liu, Yubo Liu, Xiaowei Pei, Bo Yu, Yang Wu, Lijia Liu, Chunhong Zhang, Feng Zhou "Transparent hydrophilic-oleophobic waterborne coating for multifunctional applications" Progress in Organic Coatings, Volume 191, 108454 (2024)
4. Jing Wu, Shuqing Xiang, Ming Zhang, Ninglin Zhou, Mingqian Wang, Li Li, Jian Shen "Self-Assembled Nanoflowers Realizes Synergistic Sterilization with Photothermal and Chemical Kinetics Therapy" Langmuir, 40, 5, 2591–2600 (2024)
5. Peter Hess "Group–XB Transition-Metal Dioxide and XB Dichalcogenide Monolayers" Chapter, pp 593–638, in Bonding, Structure, and Performance of Two-Dimensional Materials (2025)
6. Jiao Chen, Zonglin Gu "Molecular landscape of robust membrane disruption by Janus MoSSe nanosheet" Colloids and Surfaces B: Biointerfaces, Volume 254, 114840 (2025)
7. Tresserras Gonzalo, Bernat. "Mechanical exfoliation and characterization of 2D materials." BS thesis, Uni Barcelona (2025).
8. Akram Seifi, Hossien Riahi-Madvar & Mumtaz Ali "Progress and Future Trends of E. coli Removal from Water Environment Sources using Antibacterial Activity of Photocatalytic Coated-Surfaces: A Comprehensive Review" Water, Air, & Soil Pollution, Volume 237, article number 93 (2026)

N. Minev, K. Buchkov, N. Todorova, R. Todorov, V. Videva, M. Stefanova, P. Rafailov, D. Karashanova, Hr. Dikov, C. Trapalis, S. H. Lin, D. Dimitrov and V. Marinova "Atmospheric

pressure TAC synthesis of 2D $PtSe_2$ layers and their integration in near infrared light shutters" ACS Omega 2024, 9, 14874−14886 (2024) https://doi.org/10.1021/acsomega.3c08235

1. Qianyong Zhang, Jing Wang, Guoshun Li, Jinhu Wang, Xiuhui Yue, Heze Guo, Kai Jiang, Wei Xia and Wenjing Tang "Optimized-selenization preparation and laser Q-switching characteristics of layered $PtSe_2$" Mater. Res. Express, 11, 105009 (2024)
2. Yimin Lu, Manman Xu, Yaoyu Hu, Lin Xi, Chunlai Yang "Synthesis of the infrared transparent and conductive DLC coating based on PLD" Infrared Physics & Technology, Volume 151, 106069 (2025)
3. Mengyu Ge, Shaoqiu Ke, Shengyan Zu, Jinyu Kang, Xiaohuan Wei, Zikai Lin, Xindi Zhang, Zhiwei Huang, Guanzhou Liu, Jinrong Zhou, Jinfu Lin, Fangbiao Li, Shaoying Ke "Polarization-Encoded Transmission Enabled by $PtSe_2$/Si PIN Photodetectors with Circular Groove Light-Trapping Architecture" Advanced Functional Materials, e19663 (2025)

References:

[1] M. Snure, MJ Motala, TA Prusnick, EM Smith, D. Moore, C. Muratore, SR Vangala, NR Glavin, Two step synthesis of ultrathin transition metal tellurides, J. Vac. Sci. Technol. A. 40 (2022). https://doi.org/10.1116/6.0001893.

[2] M. O'Brien, N. McEvoy, C. Motta, JY Zheng, NC Berner, J. Kotakoski, K. Elibol, TJ Pennycook, JC Meyer, C. Yim, M. Abid, T. Hallam, JF Donegan, S. Sanvito, GS Duesberg, Raman characterization of platinum diselenide thin films, 2D Mater. 3 (2016) 1–7. https://doi.org/10.1088/2053-1583/3/2/021004.

[3] GE Jellison, FA Modine, Parameterization of the optical functions of amorphous materials in the interband region, Appl. Phys. Lett. 69 (1996) 371–373. https://doi.org/10.1063/1.118064.

[4] A. Redinger, S. Siebentritt, Loss Mechanisms in Kesterite Solar Cells, Copp. Zinc Tin Sulfide-Based Thin-Film Sol. Cells. 627 (2015) 363–386. https://doi.org/10.1002/9781118437865.ch16.

[5] J. Xie, D. Zhang, X.-Q. Yan, M. Ren, X. Zhao, F. Liu, R. Sun, X. Li, Z. Li, S. Chen, Z.-B. Liu, J.-G. Tian, Optical properties of chemical vapor deposition-grown PtSe 2 characterized by spectroscopic ellipsometry, 2D Mater. 6 (2019) 035011. https://doi.org/10.1088/2053-1583/ab1490.

[6] F. Zhang, B. Zheng, A. Sebastian, DH Olson, M. Liu, K. Fujisawa, YTH Pham, VO Jimenez, V. Kalappattil, L. Miao, T. Zhang, R. Pendurthi, Y. Lei, AL Elías, Y. Wang, N. Alem, PE Hopkins, S. Das, VH Crespi, MH Phan, M. Terrones, Monolayer Vanadium-Doped Tungsten Disulfide: A Room-Temperature Dilute Magnetic Semiconductor. Adv. Sci. 7 (2020). https://doi.org/10.1002/advs.202001174.

[7] J. Zou, Z. Cai, Y. Lai, J. Tan, R. Zhang, S. Feng, G. Wang, J. Lin, B. Liu, HM Cheng, Doping Concentration Modulation in Vanadium-Doped Monolayer Molybdenum Disulfide for Synaptic Transistors, ACS Nano. 15 (2021) 7340–7347. https://doi.org/10.1021/acsnano.1c00596.

[8] AD Oyedele, S. Yang, L. Liang, AA Puretzky, K. Wang, J. Zhang, P. Yu, PR Pudasaini, AW Ghosh, Z. Liu, CM Rouleau, BG Sumpter, MF Chisholm, W. Zhou, PD Rack, DB Geohegan, K. Xiao, PdSe2 : Pentagonal Two-Dimensional Layers with High Air Stability for Electronics, J. Am. Chem. Soc. 139 (2017) 14090–14097. https://doi.org/10.1021/jacs.7b04865.

[9] D. Wu, J. Guo, J. Du, C. Xia, L. Zeng, Y. Tian, Z. Shi, Y. Tian, XJ Li, YH Tsang, J. Jie, Highly Polarization-Sensitive, Broadband, Self-Powered Photodetector Based on Graphene/$PdSe_2$/Germanium Heterojunction, ACS Nano. 13 (2019) 9907–9917. https://doi.org/10.1021/acsnano.9b03994.

[10] L. Pi, C. Hu, W. Shen, L. Li, P. Luo, X. Hu, P. Chen, D. Li, Z. Li, X. Zhou, T. Zhai, Highly In-Plane Anisotropic 2D PdSe2 for Polarized Photodetection with Orientation Selectivity, Adv. Funct. Mater. 31 (2021). https://doi.org/10.1002/adfm.202006774.

[11] J. Yu, X. Kuang, J. Li, J. Zhong, C. Zeng, L. Cao, Z. Liu, Z. Zeng, Z. Luo, T. He, A. Pan, Y. Liu, Giant nonlinear optical activity in two-dimensional palladium diselenide, Nat. Commun. 12 (2021) 1–9. https://doi.org/10.1038/s41467-021-21267-4.

[12] Y.-H. Lin, H.-S. Chen, Electrically tunable-focusing and polarizer-free liquid crystal lenses for ophthalmic applications, Opt. Express. 21 (2013) 9428. https://doi.org/10.1364/oe.21.009428.

[13] C.-H. Lin, Y.-Y. Wang, C.-W. Hsieh, Polarization-independent and high-diffraction-efficiency Fresnel lenses based on blue phase liquid crystals, Opt. Lett. 36 (2011) 502. https://doi.org/10.1364/ol.36.000502.

[14] DK Yang, LC Chien, JW Doane, Cholesteric liquid crystal/polymer dispersion for haze-free light shutters, Appl. Phys. Lett. 60 (1992) 3102–3104. https://doi.org/10.1063/1.106765.

[15] BG Wu, JH Erdmann, J. William Doane, Response times and voltages for PDLC light shutters, Liq. Cryst. 5 (1989) 1453–1465. https://doi.org/10.1080/02678298908027783.

[16] A. Duparré, S. Kassam, Relation between light scattering and the microstructure of optical thin films, Appl. Opt. 32 (1993) 5475. https://doi.org/10.1364/ao.32.005475.

[17] C.-C. Hsu, Y.-X. Chen, H.-W. Li, J. Hsu, Low switching voltage ZnO quantum dots doped polymer-dispersed liquid crystal film, Opt. Express. 24 (2016) 7063. https://doi.org/10.1364/oe.24.007063.

[18] PS Drzaic, Polymer dispersed nematic liquid crystal for large area displays and light valves, J. Appl. Phys. 60 (1986) 2142–2148. https://doi.org/10.1063/1.337167.

[19] H. Ren, YH Lin, YH Fan, ST Wu, Polarization-independent phase modulation using a polymer-dispersed liquid crystal, Appl. Phys. Lett. 86 (2005) 1–3. https://doi.org/10.1063/1.1899749.

[20] H. Ren, ST Wu, Inhomogeneous nanoscale polymer-dispersed liquid crystals with gradient refractive index, Appl. Phys. Lett. 81 (2002) 3537–3539. https://doi.org/10.1063/1.1519102.

[21] CD Sheraw, L. Zhou, JR Huang, DJ Gundlach, TN Jackson, MG Kane, IG Hill, MS Hammond, J. Campi, BK Greening, J. Francl, J. West, Organic thin-film transistor-driven polymer-dispersed liquid crystal displays on flexible polymeric substrates, Appl. Phys. Lett. 80 (2002) 1088–1090. https://doi.org/10.1063/1.1448659.

[22] CG Pochi Yeh, Optics of Liquid Crystal Displays, Volume 67 (2009) 792.

[23] WL Chow, P. Yu, F. Liu, J. Hong, X. Wang, Q. Zeng, CH Hsu, C. Zhu, J. Zhou, X. Wang, J. Xia, J. Yan, Y. Chen, D. Wu, T. Yu, Z. Shen, H. Lin, C. Jin, BK Tay, Z. Liu, High Mobility 2D Palladium Diselenide Field-Effect Transistors with Tunable Ambipolar Characteristics, Adv. Mater. 29 (2017)

1–8. https://doi.org/10.1002/adma.201602969.

[24] Y. Zhao, J. Qiao, Z. Yu, P. Yu, K. Xu, SP Lau, W. Zhou, Z. Liu, X. Wang, W. Ji, Y. Chai, High-Electron-Mobility and Air-Stable 2D Layered $PtSe_2$ FETs, Adv. Mater. 29 (2017). https://doi.org/10.1002/adma.201604230.

[25] M. Hayyan, MA Hashim, IM Alnashef, Superoxide Ion: Generation and Chemical Implications, Chem. Rev. 116 (2016) 3029–3085. https://doi.org/10.1021/acs.chemrev.5b00407.

[26] K. Sunada, T. Watanabe, K. Hashimoto, Studies on photokilling of bacteria on TiO_2 thin film, J. Photochem. Photobiol. A Chem. 156 (2003) 227–233. https://doi.org/10.1016/S1010-6030(02)00434-3.

[27] K. Sunada, T. Watanabe, K. Hashimoto, Bactericidal activity of copper-deposited TiO_2 thin film under weak UV light illumination, Environ. Sci. Technol. 37 (2003) 4785–4789. https://doi.org/10.1021/es034106g.

[28] Y. Liu, J. Wen, Y. Gao, T. Li, H. Wang, H. Yan, B. Niu, R. Guo, Antibacterial graphene oxide coatings on polymer substrate, Appl. Surf. Sci. 436 (2018) 624–630. https://doi.org/10.1016/j.apsusc.2017.12.006.

[29] L. Gong, Z. Gu, Two Dimensional Transition Metal Dichalcogenides, Springer Singapore, 2019. https://doi.org/10.1007/978-981-13-9045-6.

[30] Y. So, D. Bin Yim, S. Lee, H. Lee, H. Kim, Y. Yu, C. Choi, JH Kim, Insights into the selective bactericidal activity of $W(Mo)Se_2$ nanosheets for therapy of pathogenic bacterial infections, Chem. Eng. J. 468 (2023) 143727. https://doi.org/10.1016/j.cej.2023.143727.

[31] Test Method for Antibacterial Activity of Semiconducting Photocatalytic Materials, Japan Ind. Stand. Comm. Tokyo Tokyo, Japan. (2009).

[32] GR Buettner, LW Oberley, Considerations in the spin trapping of superoxide and hydroxyl radicals in aqueous systems using 5,5-dimethyl-1-pyrroline-1-oxide, Biochem. Biophys. Res. Commun. 83 (1978) 69–74. https://doi.org/10.1016/0006-291X(78)90398-4.

[33] F. Ubaldi, F. Valeriani, V. Volpini, G. Lofrano, V. Romano Spica, Antimicrobial Activity of Photocatalytic Coatings on Surfaces: A Systematic Review and Meta-Analysis, Coatings. 14 (2024). https://doi.org/10.3390/coatings14010092.

[34] MAR Khan, MS Al Mamun, MH Ara, Review on platinum nanoparticles: Synthesis, characterization, and applications, Microchem. J. 171 (2021) 106840. https://doi.org/10.1016/j.microc.2021.106840.